Correlation of structure and ionic-conductivity in phosphate glass using MAS-NMR and impedance spectroscopy: Influence of sodium salt

Indrajeet Mandal,[1] Shweta R. Keshri,[1] Lekhan Lodhi,[2] Krishna K. Dey,[3] Manasi Ghosh,[4,*] Aswini Ghosh,[5,†] and Amarnath R. Allu[1,6,‡]

[1]*Energy Materials and Devices Division, CSIR-Central Glass and Ceramic Research Institute, 196 Raja S C Mullick Road, 700032 Kolkata, India*

[2]*Department of Zoology, Dr. Harisingh Gour Central University, Sagar 470003, India*

[3]*Department of Physics, Dr. Harisingh Gour Central University, Sagar 470003, India*

[4]*Physics Section, MMV, Banaras Hindu University, Varanasi 221005, India*

[5]*School of Physical Sciences, Indian Association for the Cultivation of Science, Kolkata 700032, India*

[6]*Academy of Scientific and Innovative Research (AcSIR), CSIR-Human Resource Development Centre, Ghaziabad 201002, India*

(Received 8 July 2022; accepted 13 October 2022; published 9 November 2022)

In the process of diminishing the safety concerns of sodium-ion batteries, the development of glass-based solid electrolyte materials has received adequate interest. Nevertheless, achieving a high ionic-conductivity at room temperature for glass materials remains a challenging task because of the poor correlation between the conductivity and the glass structure. Here, we attempt to understand the effective influence of NaCl on the structure and ionic-conductivity of the phosphate-based glass network. For this study, xNaCl-(100-x) (31.725 Na_2O-12.69 Al_2O_3-31.725 P_2O_5-8.46 NaF-5.40 Na_2SO_4-10 MoO_3) glass systems (mol %) were selected, where $x = 0$, 5, 10, 15, and 20 mol %. To investigate structural changes with the addition of different NaCl concentrations, ^{27}Al, ^{23}Na, ^{31}P magic angle spinning nuclear magnetic resonance (MAS-NMR), ^{31}P two-dimensional (2D) phase-adjusted spinning sideband (PASS), and ^{31}P 2D J-resolved NMR techniques and Raman spectroscopic techniques were utilized. Impedance spectroscopy and ac conductivity spectra were used to assess ionic-conductivity and sodium-ion dynamics, respectively. Impedance spectral analysis reveals that the ionic-conductivity of the base glass is increased by 2.4 times (from 1.85×10^{-7} to 4.44×10^{-7} S/cm at 373 K) with the addition of 20 mol % of NaCl. Raman spectra confirm the presence of P−O−Mo and the absence of Mo−O−Mo bonds in these glass systems, and ^{31}P 2D J-resolved spectra indicate the absence of P−O−P bonds. Upon increasing the NaCl concentration, significant changes in the shapes of ^{31}P and ^{27}Al MAS-NMR spectra were observed, indicating the effective influence of NaCl on the distribution of alumina and phosphorus structural units. Irrespective of the temperature, sodium-ion dynamic studies show that the mean-square displacement $\langle R^2(t_p)\rangle$ decreases with increasing NaCl concentration up to 10 mol % and then increases with a further increase in NaCl concentration. This investigation aids in understanding the sodium-ion dynamics and the structural information of a multicomponent glass system to enhance the room-temperature conductivity.

DOI: 10.1103/PhysRevMaterials.6.115403

I. INTRODUCTION

Due to their simple structure, mechanical reliability, safety, and high ionic-conductivity, all-solid-state batteries (ASSBs) employing solid electrolytes have received significant research interest for their application in electric vehicles, which are in huge demand at present [1,2]. Two basic types of solid electrolytes, namely sulfides and oxides, are being considered as promising electrolytes for ASSBs [3,4]. However, inorganic oxide/sulfide electrolyte materials have not yet come forward for practical applications due to their low ionic-conductivity compared to that of organic liquid electrolytes. The ionic-conductivity of sulfide-based electrolyte materials is higher than that of oxide electrolyte materials. This is because of the weaker attraction between highly polarizable sulfide networks and monovalent mobile cations as compared to the interaction between oxide networks and mobile cations [5,6]. However, sulfide-based electrolyte materials generate poisonous hydrogen sulfide upon exposure to air, and they are chemically unstable [4]. Therefore, special attention has been given to the development of oxide-based solid electrolyte materials. Moreover, oxide-based inorganic solid electrolyte materials demonstrate a high degree of safety and a wide electrochemical potential window as compared to sulfide electrolyte materials [7,8].

Among the various oxide materials, phosphate glass materials show a high potential for application as solid electrolytes in ASSBs because of their easy synthesis, high thermal expansion coefficients, low melting temperature, low softening temperature, low glass-transition temperature [9,10], and high chemical and thermal stability. Moreover, phosphate glass materials are able to accept a high concentration of various oxide components [11–13]. Therefore, phosphate-glass-based solid electrolyte materials have become a focus

*Corresponding author: manasi.ghosh@bhu.ac.in
†Corresponding author: sspag@iacs.res.in
‡Corresponding author: aareddy@cgcri.res.in

of research in the field of all-solid-state batteries. However, the major restrictions for glass electrolyte materials are their low ionic-conductivity at room temperature and the poor electrode/electrolyte interface, and these restrictions need to be addressed.

It is well documented that the ionic-conductivity of phosphate glasses is highly dependent on the network structure of the glass and the concentration of mobile cations. The correlation between the glass structure and conductivity has been poorly documented; however, it has gained momentum in the recent era due to the significant progress in the utilization of structural techniques. Solid-state nuclear magnetic resonance (SS-NMR), or the magic angle spinning nuclear magnetic resonance (MAS-NMR) spectroscopic technique, has been considered to be a key methodology for elucidating the structure of glasses at both short- and intermediate-range orders, respectively [10,14–16]. MAS-NMR for a specific nucleus is highly sensitive to its coordination number and the type of atoms in the coordination sphere of the nucleus [17]. It should be highlighted that variations in the ionic-conductivity of several glass materials with modifications in the chemical compositions have been elucidated with the help of MAS-NMR measurements [18,19]. Ogiwara, Echigo, and Hanaya [19] have utilized the ^{7}Li MAS-NMR technique to understand the variations in the Li^{+} ionic-conductivity in the LiCl-Li_2O-P_2O_5 system, and they observed that, in the high LiCl composition range, the formation of amorphous LiCl aggregate regions contributes to fast ion conduction. Combining the impedance spectroscopy and ^{7}Li MAS-NMR technique for 0.33 LiI + 0.67 Li_3PS_4 glass systems, it has been found that the formation of monovacancies in the bulk amorphous phase due to annealing enhances the ionic-conductivity [20].

To attain high ionic-conductivity for glass materials, several glass compositions have been formulated and modified in a more systematic manner. For example, Zhang, Ren, and Hu [12] have reported that the ionic-conductivity of phosphate glasses is enhanced by increasing the concentration of MoO_3 in the glass system of 20LiCl-40Li_2O-(80-x)$PO_{5/2}$-$x$$MoO_3$ ($x = 0$, 10, 20, 30, 40, 50, 60, and 70 mol %). The increase in conductivity with the increase in the concentration of MoO_3 from 0 to 20 mol % was attributed to the conversion of dimer phosphorus units into orthophosphate units, whereas the increase in the ionic-conductivity of glasses for a higher concentration of MoO_3 (30–70 mol %) was attributed to the increase in mobile cation concentrations in the molybdenum-rich phases. It has been found that with the addition of a low concentration of MoO_3 in the phosphate glasses, as-formed Mo^{6+} cations integrate with the phosphate network through P−O−Mo bonds and avoid phase separation [21,22]. Because it is a transition metal, the presence of MoO_3 in alkali-containing phosphate glasses influences not only the mobility of alkali cations but also the conduction mechanism by introducing mixed ion-polaron conductivity [23]. However, such conductivity has not been observed in 40 Na_2O-$x$$MoO_3$-(60-$x$)$P_2O_5$ glasses, where x varies from 0 to 50 mol % [24,25]. Furthermore, the increase in conductivity with increasing MoO_3 from 0 to 30 mol % in 40 Na_2O-$x$$MoO_3$-(60-$x$)$P_2O_5$ glasses is attributed to the increasing formation of P−O−Mo bonds. It has also been reported that the electronic contribution in the total conductivity is significantly low for phosphate glasses containing $MoO_3 > 15$ mol % [9,25]. A significant enhancement in ionic-conductivity has been achieved with the addition of ionic salts such as halides and sulfates [11,26–29]. The addition of LiCl to the Li_2O-P_2O_5 glass system enhances the ionic-conductivity due to the creation of a wider channel for the movement of Li^{+} ions and to the enhanced contribution of Cl in the coordination of the Li atom [26,27]. Rodrigues, Limbach, Souza, Ebendorff-Heidepriem, and Wondraczek [11] have observed that the addition of NaCl to the $NaPO_3$ glass system enhances the ionic-conductivity due to the increase in mobility of Na^{+} cations. It has been noted that the addition of halogen to chalcogenide-based solid-state electrolytes plays a significant role in enhancing ionic-conductivity [30,31]. However, much less information is available about the effective influence of NaCl on the ionic-conductivity of multicomponent phosphate glasses containing MoO_3. Moreover, the addition of NaCl also enhances the concentration of mobile cations, which is primarily responsible for the enhancement in the ionic-conductivity of glass-based ion-conducting materials. Therefore, the present study may provide a new understanding for the development processes of glass-based solid electrolytes.

In the present study, we aim to understand the effective influence of NaCl on the multicomponent phosphate glass network structure, and to correlate the structure and ionic-conductivity of the phosphate glass system. Several phosphate glasses containing multiple components, varying from three to five, have been studied extensively by doping the various additional components for the enhancement of the ionic-conductivity values [32,33]. Nevertheless, it has been identified that, in most of the cases, the effective influence of additive components on the ionic-conductivity is significant. For example, the addition of 6 mol % of Na_2SO_4 to [37.50 Na_2O-10 NaF-15 Al_2O_3-37.50 P_2O_5(mol %)] glass [32] has increased the ionic-conductivity at 373 K from 3.42×10^{-8} to 2.78×10^{-7} S/cm. Therefore, considering the effective influence of both MoO_3 and NaCl, we have chosen the complex xNaCl-(100-x) (31.725 Na_2O-12.69 Al_2O_3-31.725 P_2O_5 -8.46 NaF-5.40 Na_2SO_4-10 MoO_3) glass systems (mol %) where $x = 0$, 5, 10, 15, and 20. MAS-NMR spectroscopy, including ^{27}Al, ^{31}P, ^{23}Na, ^{31}P two-dimensional (2D) phase-adjusted spinning sideband (PASS), ^{31}P 2D J-resolved, and Raman spectroscopic techniques, has been utilized to study the structural variation with the addition of different concentrations of NaCl. The ionic-conductivity and the sodium ion dynamics have been assessed by analyzing ac-impedance spectroscopy. This investigation improves our understanding of how the sodium ion dynamics and the conductivity of a multicomponent glass system depends on its structure, and it provides guidance towards designing novel glass systems that have a high ionic-conductivity suitable for an electrolyte in sodium-ion batteries.

II. EXPERIMENTAL DETAILS

The details of the chemical compositions of the glasses considered for the present study are presented in Table I. Glasses are labeled according to the concentration

TABLE I. Chemical composition of glasses (mol %).

Sample	P_2O_5	Al_2O_3	MoO_3	Na_2O	NaF	Na_2SO_4	NaCl
Cl-0	31.73	12.69	10.00	31.73	8.46	5.40	0.00
Cl-5	30.14	12.06	9.50	30.14	8.04	5.13	5.00
Cl-10	28.55	11.42	9.00	28.55	7.61	4.86	10.00
Cl-15	26.97	10.79	8.50	26.97	7.19	4.59	15.00
Cl-20	25.38	10.15	8.00	25.38	6.77	4.32	20.00

of NaCl in the chemical composition. High-purity powders of NH_6PO_4 (99.9%, Sigma Aldrich), Al_2O_3 (99.9%, Sigma Aldrich), Na_2CO_3 (99.9%, Sigma Aldrich), NaF (98%, Merck), Na_2SO_4 (99.9%, Sigma Aldrich), NaCl (99%, Sigma Aldrich), and MoO_3 (99.97%, Sigma Aldrich) were used as raw materials for the preparation of 30 g of a homogeneous batch. In the present study, all the glasses were prepared using the melt-quench technique. The glass batches were melted in an electric furnace at a temperature of 1000 °C in alumina crucibles. It should be noted that a small concentration of Al_2O_3 leaching due to the usage of an alumina crucible should not be neglected [34]. To produce glasses in bulk form, the melts were first poured into a preheated bronze mold and then transferred to an annealing furnace at ∼350 °C. Bulk glasses with different NaCl concentrations were cut into small round pieces and polished well to achieve an optical grade finish. The dimensions were then measured using a high-precision Digital Vernier Caliper for the purpose of data analysis. Raman spectroscopic studies for all glasses were conducted using a Horiba LaBRam HR Evolution Raman spectrometer under a 488 nm Ar ion laser of 20 mW power. Furthermore, a PGSTAT12/30 differential electrometer was used to measure the electrochemical impedance spectra using a sinusoidal alternating voltage of amplitude 0.3 V in the frequency range of 0.1-10^5 Hz. This experiment was performed in an air atmosphere using two platinum meshes in a temperature range of 348–473 K.

^{31}P, ^{27}Al, and ^{23}Na MAS-NMR spectra, 2D-PASS solid-state nuclear magnetic resonance (SSNMR) spectra [35,36], and ^{31}P J-resolved NMR spectra for all glass samples were obtained using a JEOL ECX 500 MHz (11.7 T) NMR spectrometer equipped with a 3.2 mm double-resonance probe, operating at 500 MHz ^{1}H observation frequency at 297 K. Further experimental details of ^{31}P 2D-PASS measurements are provided in the Supplemental Material [37] (see also Refs. [32,35,36,38–46] therein).

The ^{31}P Larmor frequency was 202.5 MHz. The MAS frequency for the J-resolved experiment used was 10 kHz, and a 90° pulse length of ^{31}P was 3 μs. In all J-resolved investigations, a recycle delay of 200 s was used with 64 data points in indirect dimensions. The ^{31}P chemical shift was referenced by a secondary reference of 85% H_3PO_4 solution at peak position 0 ppm for ^{31}P.

A Hahn spin-echo decay pulse sequence, $(90°)_x$-τ-$(180°)_y$-τ-*acquire*, and variable dephasing times (2τ) were utilized to measure the ^{23}Na homonuclear dipolar second moment (M_2). The 90° and 180° pulse lengths were 22 and 44 μs, respectively. A ^{23}Na pulse was optimized in such a way that it only excited the central transition and did not affect satellite transitions. ^{23}Na spectra were referenced with respect to 1 M NaCl solution. Depending on the signal-to-noise ratio, 16 transients with a relaxation delay of 10 s were averaged for each data point. For each sample, 40 data points were recorded with different 2τ values. Usually, the echo that forms at τ succeeding the final 180° refocusing pulse decreases with increasing dephasing time because of homonuclear Na-Na dipole interactions [47]. Heteronuclear dipolar interactions do not contribute to the echo decay because this type of interaction is expected to be refocused in this sequence. M_2 measurement is known to be reliant on the pulse power employed and the radio rf field inhomogeneity [48]. The ^{23}Na M_2 was evaluated using the following equation [49]:

$$\frac{I\,(2\tau)}{I(0)} = \exp[-M_2(2\tau)^2/2], \tag{1}$$

where $I(2\tau)$ is the echo amplitude for the dephasing time τ, and $I(0)$ represents the echo amplitude for no dephasing.

III. RESULTS

A. Raman spectroscopy

In alkali aluminophosphate glasses, various phosphorus tetrahedral units are generally represented using $Q^n(m\text{Al})$ units, where n is the number of bridging oxygen connected to the neighboring phosphorus tetrahedral units, and m is the number of oxygens connected to aluminum tetrahedral units. It should be noted that, due to the large Raman scattering efficiency of Mo−O bond vibrations compared to the vibrations of P−O bonds, the area present in Table II may not replicate the true fraction of structural units present in the glass materials. Raman spectra for all the glasses in our present study in the range of 200–1400 cm^{-1} are depicted in Fig. 1(a). Further, the Raman spectra for all glass samples in the higher-frequency region ranging from 700 to 1300 cm^{-1} were deconvoluted to identify the structural variations in Cl-0 glass with the addition of NaCl, and the decomposed curves along with the simulated Raman spectra are shown in Fig. 1(b). The peak positions of the decomposed curves for all the glasses after the implementation of deconvolution of Raman spectra are tabulated in Table II. It is well known that the vibrational intensity of bands corresponding to Mo−O symmetric stretches is dominant in the Raman spectra of phosphate glasses due to the large Raman scattering efficiency of Mo−O bond vibrations as compared to that of P−O bonds [50–52]. Therefore, Raman spectra for all the glasses show a dominant peak at around ∼920 cm^{-1} corresponding to the stretching vibrations of Mo−O bonds. The Raman spectrum of the MoO_3 free glass (FS-6) is shown in Fig. S1 of the supplemental material for comparison [32]. The two Gaussian peaks located at 904 and 927 cm^{-1} are ascribed to O−Mo−O symmetric stretching vibrations located in tetrahedral MoO_4 units and terminal oxygen of Mo−O$^-$ of octahedral MoO_6 units, respectively [29,52,53]. The Raman band that appears at ∼390 cm^{-1} is attributed to the stretching mode of Mo−O−P bonds. This indicates that MoO_6/MoO_4 units are interlinking with PO_4 tetrahedral units through Mo−O−P bridges [53,54]. The peak appearing at ∼991 cm^{-1} corresponds to the sym-

TABLE II. Peak positions after the deconvolution of Raman spectra in the range of 700–1300 cm^{-1}. Values in parentheses represent the area of the peak in percentages.

Peak assignment	FS-6*	Cl-0	Cl-5	Cl-10	Cl-15	Cl-20
Q^2: P-O-P	721(2%)					
Q^1: P-O-P	757(4%)	758(6%)	765(7%)	763(6%)	760(6%)	760(6%)
MoO_4: O-Mo-O		904(34%)	899(39%)	898(40%)	896(40%)	895(40%)
MoO_6: Mo-O^-		927(11%)	925(17%)	923(17%)	919(17%)	918(17%)
SO_4^{2-}	988(4%)	992(3%)	990(3%)	990(3%)	989(3%)	989(3%)
Q^0(2Al)	997(15%)					
Q^0(3Al)	1040(27%)	1054(20%)	1047(13%)	1044(11%)	1045(13%)	1048(14%)
Q^1(1Al)	1108(16%)	1118(6%)	1110(6%)	1106(7%)	1111(4%)	1114(3%)
Q^2(0Al)	1182(3%)	1194(7%)	1192(5%)	1196(4%)	1182(5%)	1178(5%)
Q^2(1Al)	1222(3%)					

*Data for FS-6 glass [Ref. [40]] are included for comparison.

metric stretching vibrations of SO_4^{2-} sulfate structural units charge-compensated by the Na^+ cations. The Raman bands observed at ∼1050, ∼1118, and ∼1195 cm^{-1} are attributed to the symmetric stretching vibrations of terminal P−O^- linkages located in Q^0(2 or 3Al), Q^1(0 or 1Al), and Q^2(0Al) phosphorus structural units, respectively [55,56]. The bands at 750 and 630 cm^{-1} correspond to the symmetric stretching vibrations of bridging oxygens of P−O−P bonds in phosphorus Q^1 units and bending vibrations of P−O−Al units, respectively [57].

Upon increasing the addition of NaCl, peaks of both O−Mo−O and Mo–O^- vibrations shift towards the lower wave number [Fig. 1(b)]. This could be attributed to structural variation around the molybdenum structural units. Figures 1(a) and 1(b) clearly disclose the appearance of a high-intensity peak at ∼904 cm^{-1} for Cl-20 glass. This indicates the increasing concentrations of O−Mo−O linkages with increasing the NaCl concentration and consequently the increase in the concentration of MoO_4 structural units at the expense of MoO_6 units. Chowdari, Tan, and Chia [58] have also reported the conversion of MoO_6 units into MoO_4 units by increasing the concentration of Li_2O in the Li_2O-MoO_3-P_2O_5 glass system. Moreover, it has been reported from the ^{95}Mo NMR studies [59] for (100-x)$NaPO_3$-$x$$MoO_3$ glass samples that most of the molybdenum exists in fourfold-coordination states in the samples containing molybdenum at low to medium concentration, i.e., up to 45 mol %.

Figures 1(a) and 1(b) show that the intensity of the peaks at ∼1050, ∼1118, and 750 cm^{-1} decreases significantly with increasing NaCl concentration, indicating a decrease in the concentration of Q^1(0Al) and Q^0(2 or 3Al) structural units. This finding indicates that successive depolymerization of the glass network increases with increasing the NaCl concentration. This is in accordance with the studies reported by Rodrigues, Limbach, Souza, Ebendorff-Heidepriem, and Wondraczek [11] for the $NaPO_3$-NaCl glass system, and by Rao and Seshasayee [27] for the Li_2O-P_2O_5-LiCl glass system. Significant variation either with the peak position or the

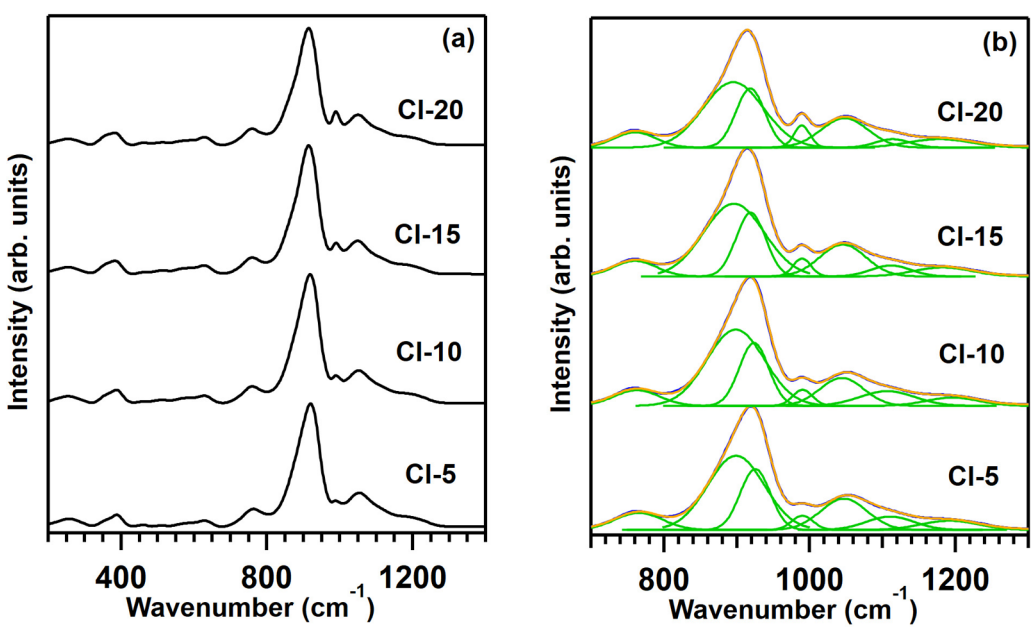

FIG. 1. (a) Raman spectra of glasses and (b) deconvolution of Raman spectra of glasses in the range of 700–300 cm^{-1}.

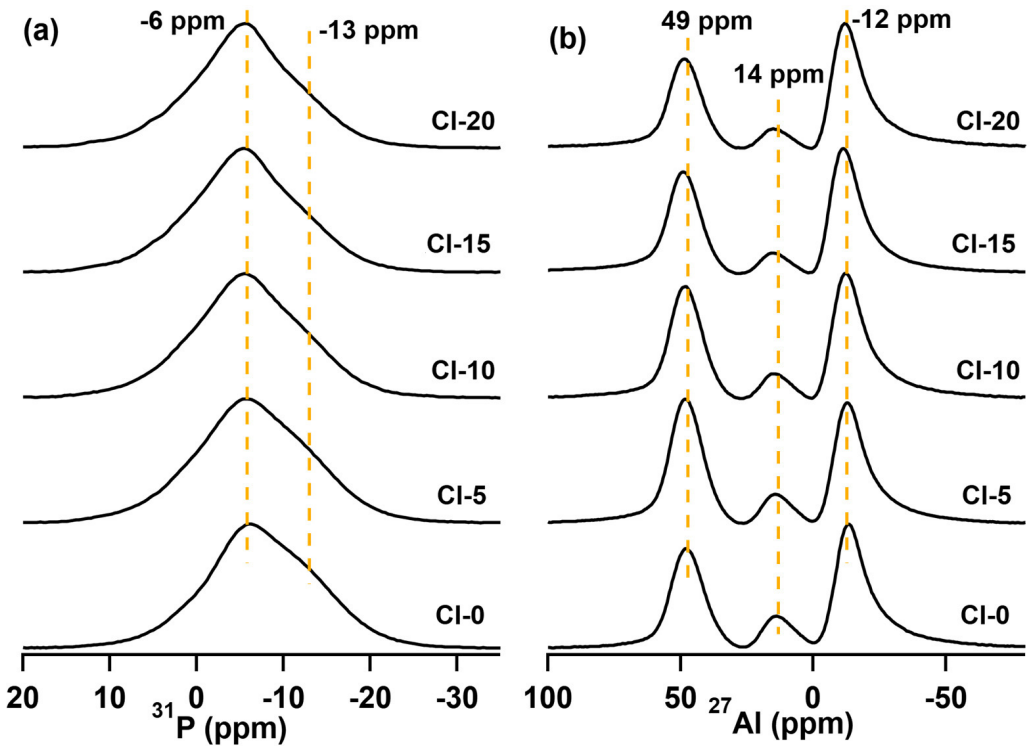

FIG. 2. (a) ^{31}P and (b) ^{27}Al MAS-NMR spectra. All spectra were recorded with a MAS frequency of 18 kHz and with a short excitation pulse.

intensity of the peak at 991 and 570 cm^{-1}, which is related to $Al(O,F)_6$ structural units, is not observed with the addition of NaCl. The absence of symmetric stretching vibrations of Mo−O−Mo linkages, which results in a Raman band at around ∼840 cm^{-1}, indicates that molybdenum clusters are not formed within the compositional range considered for the present study [52,59].

B. MAS-NMR

1. ^{31}P MAS-NMR spectra

Figure 2(a) depicts the ^{31}P MAS-NMR spectra for all the glasses. All the spectra display a broad and asymmetric signal with a full width at half-maximum of >15 ppm. The broad resonance spectra highlight the superimposition of signals arising due to the presence of various structural units with close chemical shifts [13,60]. The Cl-0 glass spectrum has a single high-intensity peak located at around −6 ppm with a small hump located at around −13 ppm in the lower chemical shift region. The chemical shifts at appearing at −6 and −13 ppm are characteristic chemical shifts of Q^0(2Al) and Q^0(3Al) units in sodium aluminophosphate glasses [61,62]. The spectrum of Cl-0 glass is more analogous to the FS-6 glass spectrum [32], except for the reduced intensity of the peak at around −13 ppm in Cl-0 glass. This indicates that the addition of MoO_3 depolymerizes the phosphate network of FS-6 glass through the substitution of P−O−Al/P−O−P bonds with P−O−Mo bonds [63]. This is consistent with results reported for the $40\,Na_2O$-$(60$-$x)P_2O_5$-$xMoO_3$ glass system [24]. Tricot, Tayeb, Koudelka, Mosner, and Vezin [13] have also reported that the Mo^{6+} ions at their high concentration in the mixed borophosphate network attract the phosphorus from the borophosphate network and form the P−O−Mo bonds. Furthermore, with the progressive addition of NaCl, a high-intensity peak position (−6 ppm) in the spectrum of Cl-0 glass is shifted slightly towards higher chemical shifts; nevertheless, the shape of the peak changes moderately. The most apparent change in the shape of the spectrum is the decrease in the intensity of the hump in the lower chemical shift region [Fig. 2(a)]. This result is more analogous to the results observed for the aluminophosphate glasses containing a high Na/P ratio [64]. This indicates that the increase in NaCl concentration disrupts the phosphorus tetrahedral units that are associated with large numbers of alumina tetrahedral units, and it creates a greater number of nonbridging oxygens. Due to the complexity in the chemical composition of the glass systems used in the present study, it may be noted that the observed chemical shift at around −6 ppm can also be due to the presence of Q^1(1Al) phosphorus structural units [32,33]. Nevertheless, the more asymmetric nature of 1D ^{31}P MAS-NMR spectra cannot be completely resolved. Therefore, to obtain further accurate information about the $Q^n(m\mathrm{Al})$ units, 2D-PASS and J-resolved experiments were utilized. These methods disclose the distinction between P−O−P and those devoid of P−O−P linkages [65].

The representative ^{31}P 2D-PASS MAS-NMR spectrum for the Cl-5 glass is shown in Fig. 3. The 2D PASS SS-NMR experiment has been applied on different types of glasses by different groups to extract chemical shift anisotropy (CSA) tensors of ^{29}Si, ^{31}P, and ^{119}Sn nuclei. In the case of MAS-NMR, the different $Q^0(m\mathrm{Al})$ species are distinguished based on the isotropic chemical shift of ^{31}P. Nevertheless,

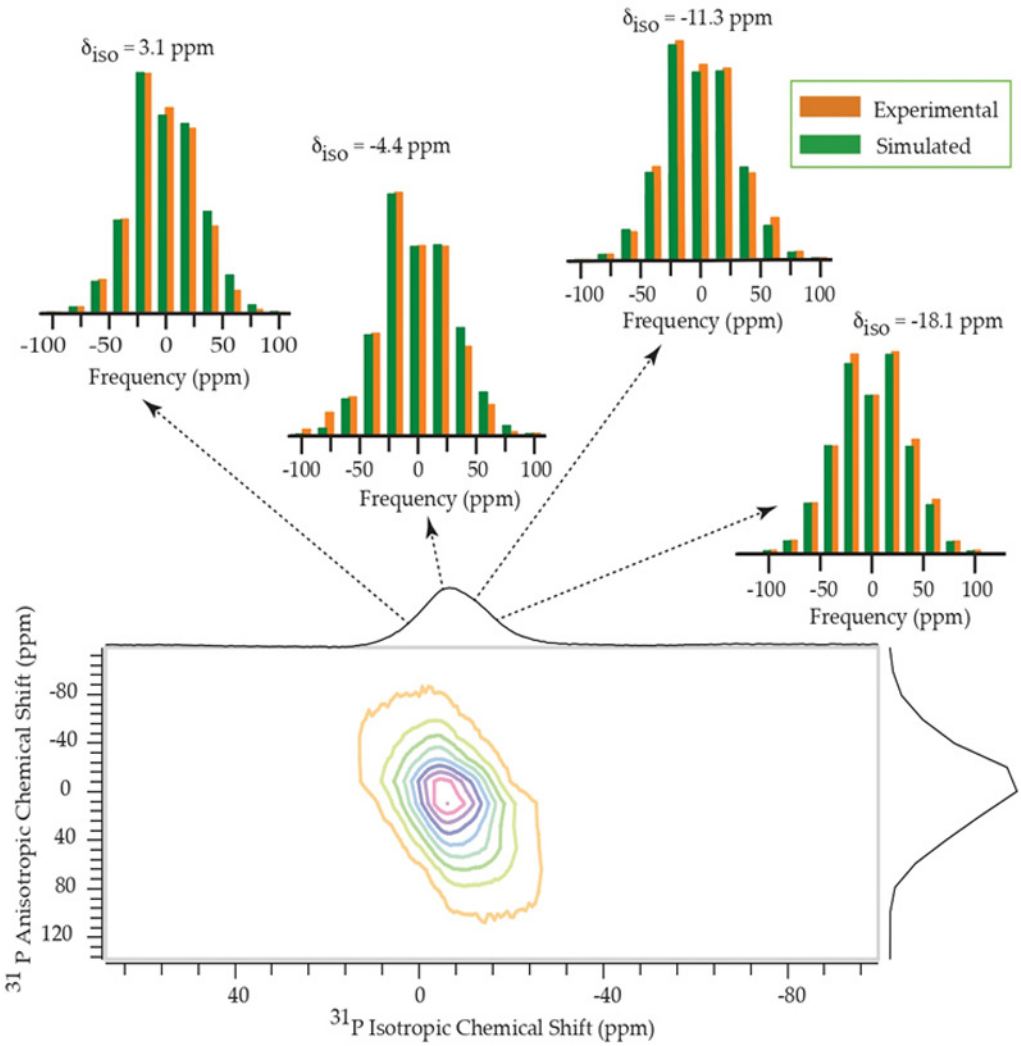

FIG. 3. ^{31}P 2D PASS MAS NMR spectrum of Cl-5 glass. The spinning CSA sideband pattern corresponding to the position of isotropic chemical shift 3.1 ppm, −4.4 ppm, −11.3 ppm, and −18.1 ppm is also shown in the figure.

isotropic chemical shifts can mislead the assignment of different $Q^0(m\text{Al})$ species. Therefore, with the knowledge of CSA tensors from the 2D PASS experiment, various $Q^{(n)}$ species can be assigned with more certainty. Here, the Cl-0 glass and glasses with various concentrations of NaCl were studied using ^{31}P 2D-PASS NMR. The analysis of different CSA parameters for different glasses is given in Table III, and the descriptions of parameters mentioned in Table III are included in the supplemental material [37] (see also Refs. [32,35,36,38–46] therein). The four different isotropic positions and their corresponding CSA parameters are given in Table III. Interestingly, for the Cl-0 glass sample, it is observed that although the isotropic position changes from −18.1 to 3.1 ppm (Table III), the anisotropy parameters, particularly the span and asymmetry parameters, remain unchanged. These trends are observed for all other samples (Table III). This result confirms unambiguously that all the samples contain only $Q^0(m\text{Al})$ species.

The homonuclear 2D J-resolved ^{31}P MAS NMR experiment was also conducted to verify connectivity between the different (PO_4) species through the P−O−P bond. J-resolved ^{31}P MAS NMR spectra for Cl-5 and Cl-20 glasses are shown in Fig. 4. For both Cl-5 and Cl-20 glasses, the signal components near about −30, −10, and 5 ppm in the J-resolved spectra reveal the singlets. This further indicates that the majority of the signals arise due to the presence of isolated Q^0 structural units. Overall, ^{31}P 2D-PASS and J-resolved NMR spectra confirm that the signals represented in 1D ^{31}P MAS-NMR spectra are slowly due to the Q^0(2Al) and Q^0(3Al) structural units. The presence of spectra at 5 ppm in J-resolved ^{31}P MAS NMR spectra also confirms the presence of Q^0(0Al) structural units in all the glass.

Based on the results of ^{31}P 2D-PASS NMR and homonuclear 2D J-resolved spectroscopy, 1D ^{31}P MAS-NMR spectra was deconvoluted by the DMFIT software. The decomposition figures are shown in Fig. S2 in the Supplemental Material. The results obtained from the deconvolution of ^{31}P MAS-NMR are provided in Table IV. The observed deconvolution peaks at around −18, −11, −6, and 3 ppm are assigned to Q^0(4Al), Q^0(3Al), Q^0(2Al), and Q^0(0Al) phosphorus structural units, respectively [62,66,67]. The deconvolution analysis confirms that, at the expense of Q^0(3Al) units, Q^0(2Al) and Q^0(0Al) units increase upon increasing the NaCl concentration in the Cl-0 glass.

TABLE III. Chemical shift anisotropy parameters for all the glass samples.

δ_{iso} (ppm)	δ_{11} (ppm)	δ_{22} (ppm)	δ_{33} (ppm)	Span (ppm)	Skew	Anisotropy (ppm)	Asymmetry
Cl-0							
−18.1	43.2 ± 1.0	−22.0 ± 0.7	−75.4 ± 0.7	118.6 ± 1.3	−0.1	91.9 ± 1.2	0.9
−11.3	49.9 ± 1.0	−15.2 ± 0 .7	−68.6 ± 0.7	118.6 ± 1.3	−0.1	91.9 ± 1.6	0.9
−6.1	55.2 ± 1.1	−10.0 ± 0.7	−63.4 ± 0.8	118.6 ± 1.4	−0.1	91.9 ± 1.6	0.9
3.1	62.4 ± 1.2	3.1 ± 0.8	−56.1 ± 0.9	118.6 ± 1.6	0	−88.9 ± 1.3	1.0
Cl-5							
−18.1	47.9 ± 4.5	−17.1 ± 2.7	−85.2 ± 3.6	133.2 ± 4.8	0.02	−100.5 ± 5.5	0.97
−11.3	48.5 ± 2.5	−13.9 ± 1.4	−68.4 ± 2.0	116.8 ± 2.9	−0.07	89.6 ± 3.8	0.9
−4.4	58.9 ± 2.2	−9.2 ± 1.3	−63.0 ± 1.8	121.9 ± .5	−0.11	95.0 ± 3.3	0.8
3.1	64.2 ± 2.1	−1.7 ± 1.2	−53.2 ± 1.7	117.4 ± 2.5	−0.12	91.7 ± 3.2	0.8
Cl-10							
−17.9	43.3 ± 1.4	−21.9 ± 1.0	−75.2 ± 1.0	118.6 ± 1.9	−0.1	91.9	0.9
−11.1	48.2 ± 2.7	−11.1 ± 1.8	−70.4 ± 1.5	118.6 ± 2.7	0	−88.9 ± 2.2	1.0
−5.6	53.7 ± 1.4	−5.6 ± 0.9	−64.9 ± 1.0	118.6 ± 1.9	0	−88.9 ± 1.6	1.0
3.3	66.5 ± 1.9	−4.6 ± 1.2	−52.0 ± 1.4	118.6 ± 2.5	−0.2	94.9 ± .8	0.7
Cl-15							
−18.17	41.1 ± 2.2	−18.2 ± 1.5	−77.4 ± 1.6	118.6 ± 2.9	0	−88.9 ± 1.5	1.0
−13.0	46.2 ± 1.7	−13.0 ± 1.1	−72.3 ± 1.3	118.6 ± 2.3	0	−88.9 ± 1.9	1.0
−5.5	55.8 ± 1.2	−9.4 ± 0.9	−62.8 ± 0.9	118.6 ± 1.6	−0.1	91.9 ± 1.9	0.9
3.0	64.3 ± 1.1	−0.9 ± 0.2	−54.2 ± 1.1	118.6 ± 1.3	−0.1	91.9 ± 1.4	0.9
Cl-20							
−18.3	32.7 ± 0.7	−21.6 ± 0.4	−66.0 ± 0.6	98.8 ± 1.2	−0.1	76.6 ± 1.1	0.9
−13.1	37.9 ± 0.9	−16.4 ± 0.5	−60.9 ± 0.7	98.8 ± 1.3	−0.1	76.6 ± 1.4	0.9
−5.6	43.8 ± 1.1	−5.6 ± 0.6	−55.0 ± 0.9	98.8 ± 1.8	0	−74.1 ± 1.4	1.0
3.06	64.3 ± 1.1	−0.9 ± 0.2	−54.2 ± 1.1	118.6 ± 1.3	−0.1	91.9 ± 1.4	0.9

2. ^{27}Al *MAS-NMR spectra*

^{27}Al MAS-NMR spectra are shown in Fig. 2(b). The spectra for all the glasses show three well-resolved asymmetric peaks located at 49, 14, and −12 ppm, which are undoubtedly attributed to aluminum in fourfold, fivefold, and sixfold coordination, respectively [68,69]. Comparison of these chemical shifts with the ^{27}Al MAS-NMR spectra of sodium aluminophosphate glasses highlights that the local environment of aluminum in each coordination is completely surrounded by PO_4 units [62,67]. This indicates that $Al(OP)_4$, $Al(OP)_5$, and $Al(OP)_6$ units exist in the present glass systems. It has been reported that the fluorine in the sodium aluminophosphate glasses is preferably connected to the sixfold-coordinated aluminum and forms $Al(OP, F)_6$ structural units [64,68]. Due to the overlapping chemical-shift regions for the $Al(OP)_6$ and $Al(OP, F)_6$ units, we could not

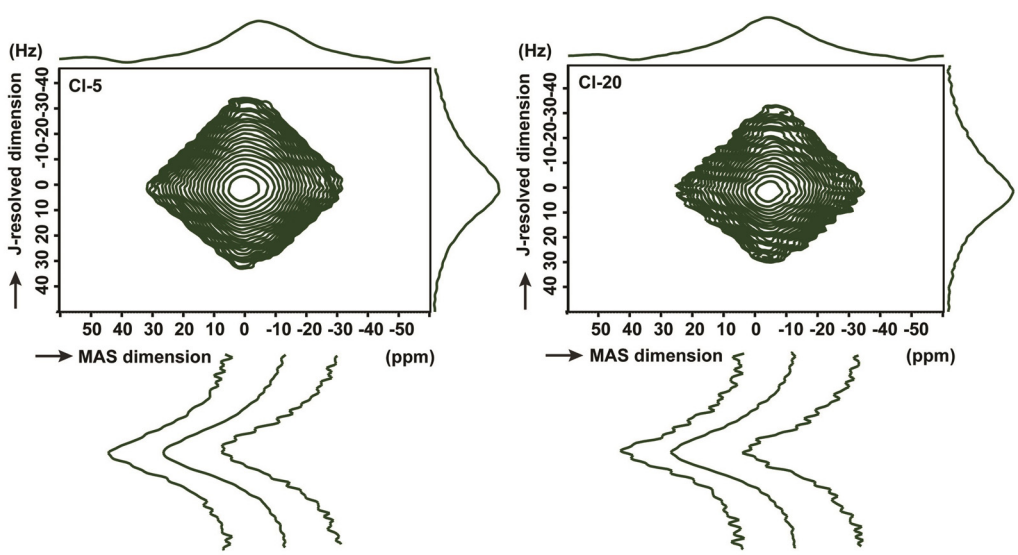

FIG. 4. J-resolved ^{31}P MAS NMR results of Cl-5 and Cl-20 glass.

TABLE IV. ^{31}P MAS-NMR deconvolution data.

Compound name	Phosphorus nuclei	Isotropic chemical shift (ppm)	Relative abundance
Cl-0	Q^0(4Al)	−18.1	2.23%
	Q^0(3Al)	−11.3	53.92%
	Q^0(2Al)	−6.1	32.97%
	Q^0(0Al)	3.1	10.88%
Cl-5	Q^0(4Al)	−18.1	4.26%
	Q^0(3Al)	−11.3	40.73%
	Q^0(2Al)	−4.4	42.43%
	Q^0(0Al)	3.1	12.53%
Cl-10	Q^0(4Al)	−17.9	3.14%
	Q^0(3Al)	−11.1	36.52%
	Q^0(2Al)	−5.6	42.41%
	Q^0(0Al)	3.3	17.93%
Cl-15	Q^0(4Al)	−18.17	0.53%
	Q^0(3Al)	−13.0	31.68%
	Q^0(2Al)	−5.5	50.87%
	Q^0(0Al)	3.0	16.92%
Cl-20	Q^0(4Al)	−18.3	2.08%
	Q^0(3Al)	−13.1	31.43%
	Q^0(2Al)	−5.6	47.17%
	Q^0(0Al)	3.06	19.33%

distinguish their presence from the simple 1D ^{27}Al MAS-NMR spectrum. Therefore, the peak observed at ∼−12 ppm is attributed to both $Al(OP)_6$ and $Al(OP, F)_6$ units [68]. Figure 2(b) and Fig. S3 in the Supplemental Material clearly show that the intensity of the peaks observed at −12 ppm is dominant, reflecting that all glasses are enriched with $Al(OP)_6$ units [67]. To identify the variations in the fraction of aluminum components, the spectrum was further decomposed into three components using the Czjzek model, and the parameters are displayed in Table V. Zhang, Araujo, and Eckert [61,64] have shown that the concentration of sixfold-coordinated aluminum decreases upon increasing the O/P ratio. It is interesting to note that the addition of 10 mol % MoO_3 to the FS-6 glass significantly enhanced the concentration of $Al(OP, F)_6$ units despite the increase in the O/P ratio from 3.94 (FS-6) to 4.41 (Cl-0) at the constant Al/P (0.4) and Na/P (1.3) ratios. This observation confirms the significant influence of MoO_3 on the coordination of aluminum, though the direct interaction between Al and Mo is not evident from the ^{27}Al MAS-NMR spectrum. It is evident from Table V that the concentration of $Al(OP)_6$ units decreases with the initial 5 mol % addition of NaCl to the Cl-0 glass, after which it reduces with the further addition of NaCl up to 20 mol %. Additionally, the concentration of $Al(OP)_4$ units increases with the initial 5 mol % NaCl addition to the Cl-0 glass and then decreases with the further addition of NaCl up to 20 mol %. Therefore, it can be inferred that the $Al(OP)_6$ and $Al(OP)_4$ units are forming at the expense of $Al(OP)_5$. In contrast, the concentration of $Al(OP)_5$ units decreases continuously with the increasing addition of NaCl content from 5 to 20 mol %. These results show that the addition of NaCl influences the environment of aluminum in the Cl-0 glass.

TABLE V. 27 Al MAS-NMR deconvolution data.

Compound name		Isotropic chemical shift (ppm)	Relative abundance	C_Q (MHz)	sCz_C_Q (MHz)
Cl-0	AlO_4	47.90	39.54%	2.80	1.40
	AlO_5	14.60	16.60%	2.80	1.40
	AlO_6	−11.40	43.86%	2.73	1.36
Cl-5	AlO_4	47.90	44.30%	2.56	1.28
	AlO_5	15.00	14.65%	2.80	1.40
	AlO_6	−10.90	41.06%	2.80	1.40
Cl-10	AlO_4	48.10	41.50%	2.56	1.28
	AlO_5	15.20	13.21%	2.66	1.33
	AlO_6	−10.20	45.29%	2.80	1.40
Cl-15	AlO_4	48.10	39.95%	2.56	1.28
	AlO_5	15.80	11.67%	2.66	1.33
	AlO_6	−9.40	48.39%	2.80	1.40
Cl-20	AlO_4	48.10	37.42%	2.56	1.28
	AlO_5	15.80	11.93%	2.66	1.33
	AlO_6	−9.60	50.65%	2.80	1.40

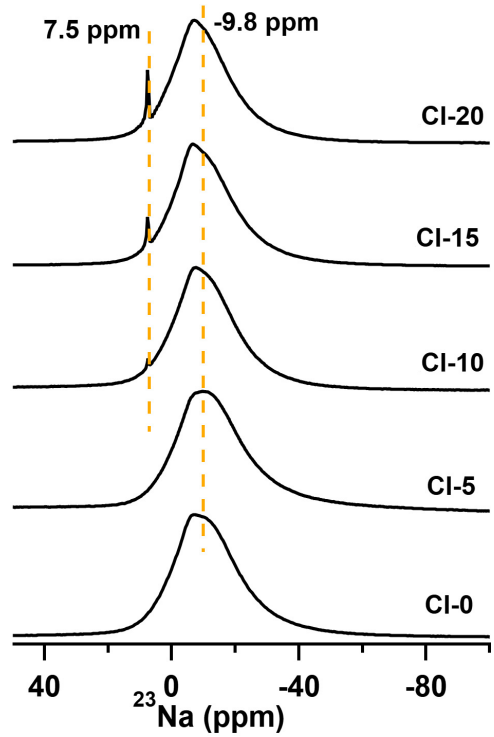

FIG. 5. ^{23}Na MAS-NMR spectra.

3. ^{23}Na *MAS-NMR spectra*

^{23}Na MAS-NMR spectra for different glasses are depicted in Fig. 5. The spectra for all glasses show a maximum resonance peak at around ∼−9.8 ppm, while an additional sharp peak appears at around 7.5 ppm for Cl-10, Cl-15, and C-20 glasses. The peak at around 7.5 ppm is attributed to the NaCl crystalline phase [70]. The intensity of the sharp peak increases with increasing NaCl concentration from 10 to 20 mol %. The NaCl crystalline phases might occur during the annealing of glass materials. The high-intensity peak position shifts towards higher chemical-shift regions with increasing NaCl concentrations. This is consistent with previous studies,

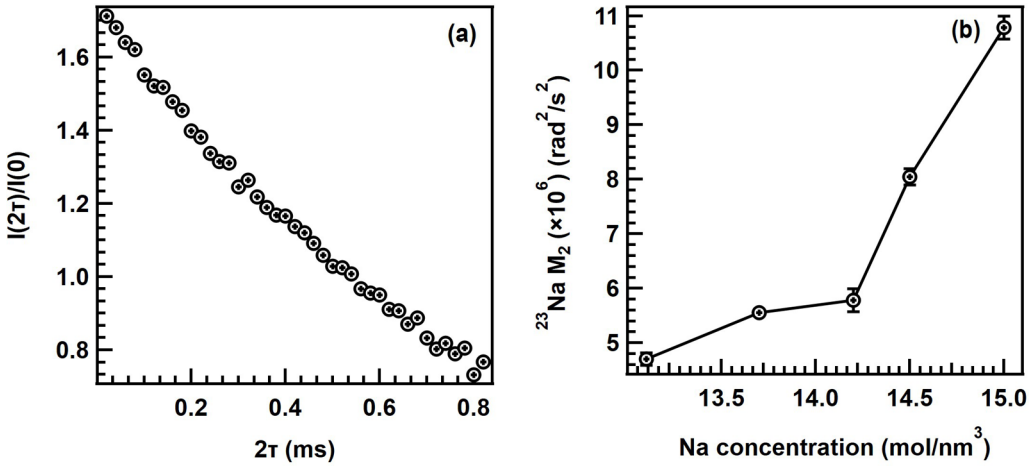

FIG. 6. (a) ^{23}Na spin-echo data for Cl-20 glass: Integrated intensity plot as a function of echo spacing (2τ) in ms. (b) The plot shows the variation of the second moment M_2 with Na concentration.

which reported that the ^{23}Na chemical shift moves towards the higher chemical shift region with increasing sodium concentrations, indicating the increased role of network modifiers in the glass systems [32,71–73]. This is further proof that the role of network modifiers increases upon increasing the NaCl concentration in Cl-0 glass in our current study.

Figure 6(a) demonstrates ^{23}Na spin-echo decay curves for the Cl-20 glass. ^{23}Na spin-echo decay curves for other glasses also show similar curves and therefore they are not shown here. The curve shown in Fig. 6(a) is then fitted with Eq. (1) to obtain the M_2 values. The M_2 values obtained for all the glasses are presented in Fig. 6(b) with respect to the variations in sodium-ion concentration. It has been observed that the trend in the variation of M_2 values with respect to sodium concentrations (N_v) reflects the spatial distribution of sodium cations [74–77]. In general, a linear correlation between M_2 and N_v indicates the random distribution of Na^+ cations, while the homogeneous distribution of Na^+ cations exhibits a parabolic correlation. Nevertheless, a constant value of M_2 against the N_v values reflects the cluster formation of Na^+ cations in the network structure of glass. Figure 6(b) shows that $M2$ is nearly constant up to 14.25 mol/nm^3 of Na concentration in the Cl-x ($x = 0, 5, 10, 15, 20$) glass system, indicating the presence of clusters of Na^+ cations. Nevertheless, the linear correlation of M_2 with the Na^+ concentration indicates the random distribution of Na^+ cations. To comment more on the spatial distribution of Na^+ cations in the Cl-0 glass containing various concentrations of NaCl, more sophisticated experiments will be necessary.

C. Electrical properties

1. dc conductivity

The impedance spectroscopy technique was utilized to measure the ionic-conductivity of transparent bulk glasses. The normalized data (impedance data have been multiplied by A/t, where A is the area and t is the thickness of the glass sample) collected from the impedance measurements are shown in Fig. 7(a) in the form of Nyquist plots for all the samples at 373 K. The Nyquist plots show a semicircle in the higher-frequency region that represents the bulk conductivity of glass material, and the spike in the lower-frequency region originates due to charge accumulation between the electrolyte

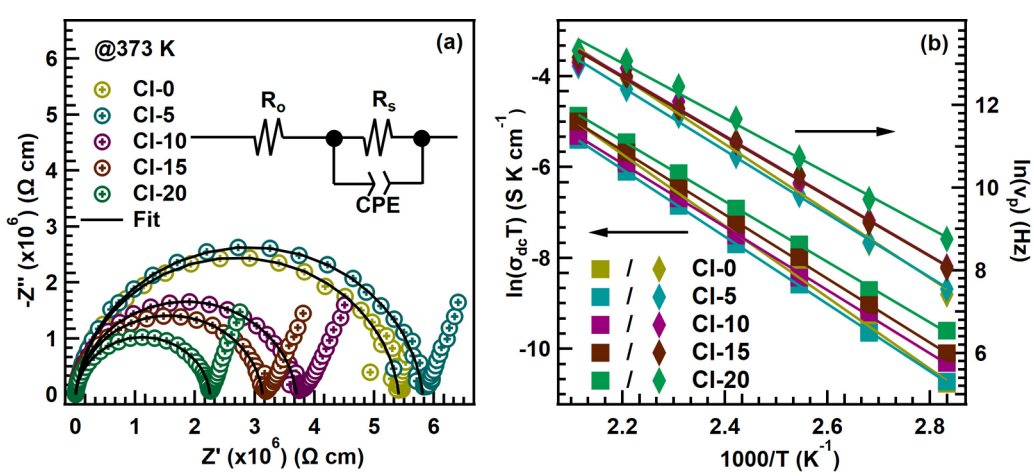

FIG. 7. (a) Nyquist plot for different glass samples at temperature 373 K. The inset shows the equivalent circuit. (b) Temperature-dependent Arrhenius plot for conductivity and crossover frequency.

TABLE VI. Conductivity and activation energy for all glass samples.

Sample	Temperature (K)	Conductivity (S/cm)	Activation energy (eV)	Activation energy for crossover frequency (eV)
Cl-0	373	$1.85 \times 10^{-7} \pm 4.88 \times 10^{-9}$	0.68 ± 0.014	0.70 ± 0.027
	473	$1.22 \times 10^{-5} \pm 3.86 \times 10^{-7}$		
Cl-5	373	$1.72 \times 10^{-7} \pm 5.58 \times 10^{-9}$	0.64 ± 0.003	0.66 ± 0.013
	473	$9.49 \times 10^{-6} \pm 3.10 \times 10^{-7}$		
Cl-10	373	$2.72 \times 10^{-7} \pm 7.36 \times 10^{-9}$	0.60 ± 0.009	0.63 ± 0.026
	473	$1.04 \times 10^{-5} \pm 3.76 \times 10^{-7}$		
Cl-15	373	$3.19 \times 10^{-7} \pm 8.13 \times 10^{-9}$	0.60 ± 0.007	0.62 ± 0.013
	473	$1.43 \times 10^{-5} \pm 4.59 \times 10^{-7}$		
Cl-20	373	$4.44 \times 10^{-7} \pm 1.20 \times 10^{-8}$	0.57 ± 0.006	0.57 ± 0.023
	473	$1.62 \times 10^{-5} \pm 5.12 \times 10^{-7}$		

and the metal electrode. To evaluate the bulk resistance of the glass samples, the Nyquist plots were fitted with an equivalent circuit consisting of resistance (R) and constant phase elements (CPE) using the ZVIEW software. The equivalent circuit diagram is shown in the inset of Fig. 7(a), where R_s is the bulk resistance and R_o is the Ohmic resistance due to the connected wires and the metal electrode. The ionic-conductivity ($\sigma_{\rm dc}$) of the bulk glasses is then calculated using the formula

$$\sigma_{\rm dc} = \frac{t}{R_s \times A} \tag{2}$$

The conductivity values measured at 373 and 473 K are given in Table VI. With the addition of 20 mol % of NaCl, the ionic-conductivity of Cl-0 glass increased from 1.85×10^{-7} to 4.44×10^{-7} S/cm at 373 K. It may be noted that the obtained values are higher than those for sodium borosilicate glasses [78].

Figure 7(b) shows the variation of the ionic-conductivity with respect to the inverse of the temperature. It clearly indicates that for all the glasses, the ionic-conductivity variation with temperatures ranging from 373 to 473 K follows the Arrhenius equation. Therefore, the activation energy (E_a) for the ionic-conductivity is calculated from the slope of Arrhenius plots using the Arrhenius equation

$$\sigma_{\rm dc} T = \sigma_0 e^{(-\frac{E_a}{k_b T})} \tag{3}$$

and the values are tabulated in Table VI. The activation energy decreases with increasing NaCl concentration in the glass sample, and the lowest activation energy of 0.57 ± 0.006 eV is observed for Cl-20 glass. Figure 7(b) shows the variation of crossover frequency with respect to the inverse of temperature. Data points for all the glasses shown in Fig. 7(b) follow a straight line and are therefore fitted with Eq. (4) to extract the activation energy for the crossover frequency (E_c),

$$\nu_p = \nu_0 e^{-\frac{E_c}{k_B T}}. \tag{4}$$

In Eq. (4), ν_p is the crossover frequency, ν_0 is the preexponential factor, E_c is the activation energy for the crossover frequency, and k_B is the Boltzmann constant. E_c for all the glass samples is tabulated in Table VI. The activation energy of the crossover frequency decreases with increasing NaCl concentration and is consistent with the activation energy obtained for the dc conductivity [Fig. 9(b)].

2. ac-conductivity spectra

To correlate conductivity with the structure of glasses and to understand ion conduction mechanisms, ac-conductivity analysis has been implemented. As an example, the real part of the ac-conductivity spectrum for Cl-10 glasses at different temperatures has been calculated from the impedance data and is shown in Fig. 8(a). Figure 8(b) shows the frequency-dependent real part (ε') of the complex dielectric constant ($\varepsilon^* = \varepsilon' - i\varepsilon''$). The electrode polarization effect, in which all the dipoles align themselves in the direction of the electric field and contribute to the total polarization, results in a higher value of the dielectric constant at lower frequencies. In contrast, the value of the dielectric constant declines and moves closer to a constant value $\varepsilon(\infty)$ in higher-frequency regions because of the rapid changes in the electric field, making it difficult for these dipoles to orient in the direction of the electric field and fully contribute to the total polarization. In the intermediate region of frequency, with increasing frequency, the variation of the dielectric constant is negligible, and it forms a plateau region that is denoted as $\varepsilon(s)$. Generally, the response of the frequency-dependent ac-conductivity is expressed using the following equation:

$$\sigma(\nu) = \left(\sigma_{\rm dc}\left(1 + \left(\frac{\nu}{\nu_p}\right)^n\right)\right) + (A\nu), \tag{5}$$

where ν_p is the crossover frequency, and A and n are constants. The first term in Eq. (5) is known as a universal dielectric response (UDR) proposed by Jonscher. The second term in Eq. (5) indicates the nearly constant loss (NCL) phenomenon, which was discovered by Nowick and co-workers [79]. The NCL effect is usually observed at temperatures below 100 K and frequencies ranging from less than 1 Hz to more than 1 MHz [80]. The NCL effect is, therefore, neglected in the present study due to high-temperature conductivity measurements. ac-conductivity spectra at different temperatures ranging from 373 to 473 K were fitted only with the Jonscher term, and the values of ν_p, σ_{dc}, and n were extracted. In general, the lower value of n indicates linear 1D motion of charged ions, and the higher value of n indicates random back-and-forth 3D motion [81]. In the present study, n values ranging between 0.78 and 0.99 indicate that the charge cations diffuse in 3D conduction paths for the present glasses.

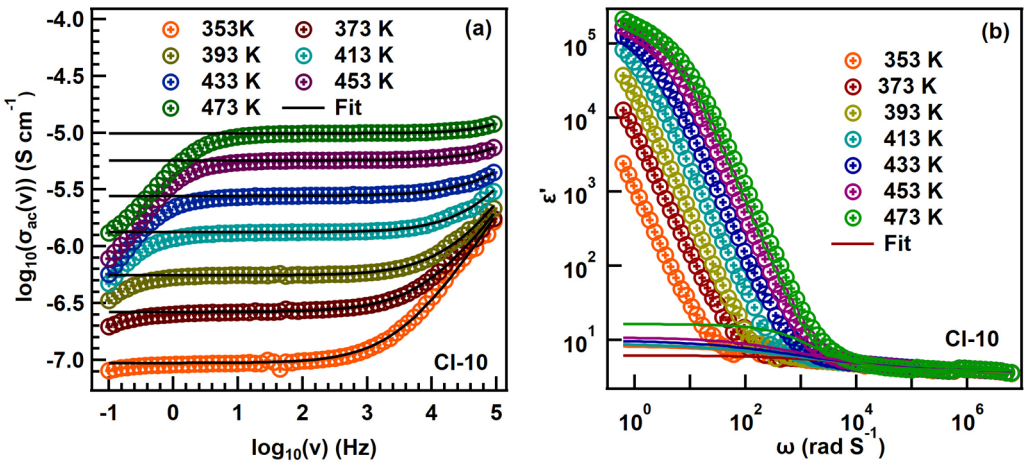

FIG. 8. (a) Conductivity variation with frequency for Cl-0 glass samples. (b) Dielectric spectra for Cl-0 glass sample at different temperatures. The solid line indicates a fitted curve.

In ion conducting glasses where the conductivity is controlled by the random hopping of charge carriers, the Nernst-Einstein relation [82] can be expressed as

$$\sigma_{\mathrm{dc}}T = K(N, q, \xi)\nu_p, \tag{6}$$

where $K(N, q, \xi) = \gamma N q^2 \xi^2/6k$ is a constant, ξ is the mean hopping distance, N is the concentration of the charge carrier, γ is the fraction of mobile cations, and k is the Boltzmann constant. As $K(N, q, \xi)$ is only proportional to N, the increase in the concentration of the charge carrier in any glass system increases the proportional constant K, and the data points in the $\log_{10}(\sigma_{\mathrm{dc}}T)$ versus $\log_{10}(\nu_{\mathrm{p}})$ curve shift towards an upward direction [83]. The $\log_{10}(\sigma_{\mathrm{dc}}T)$ versus $\log_{10}(\nu_{\mathrm{p}})$ curve for all the glass samples [Fig. 9(a)] clearly shows that the linear slopes of each curve are not superimposing with each other. The slope of the curve shifts upward with a slight deviation for Cl-15 glass. For further confirmation, we have extracted the value of $\log_{10}(K(N,q,\xi))$ from the $\log_{10}(\sigma_{\mathrm{dc}}T)$ versus $\log_{10}(\nu_{\mathrm{p}})$ curve. Variation of the proportionality constant $\log_{10}(K(N,q,\xi))$ with respect to NaCl concentration is shown in Fig. 10. Figure 10 clearly indicates that Cl-10 has the highest charge-carrier concentration, and Cl-20 has the lowest.

According to linear-response theory [84], the mean-square displacement $\langle r^2(t)\rangle$ of a charge carrier and the real part of the ac-conductivity data are related by the following relation:

$$\sigma'(\nu) = \frac{Nq^2 4\pi^2\nu^2}{6k_bTH_R}\int_0^\infty \langle r^2(t)\rangle \sin(2\pi\nu t)dt, \tag{7}$$

where k_b is the Boltzmann constant, T is the temperature, ν is the frequency, H_R is the Haven ratio, N is the charge-carrier concentration, and q is the charge of the mobile ions. Implementing the inverse Fourier transformation, Eq. (7) converts into

$$\begin{aligned}\langle r^2(t)\rangle &= \frac{12k_bTH_R}{Nq^2\pi}\int_0^t dt'\int_0^\infty \frac{\sigma'(\nu)}{\nu}\sin(2\pi\nu t')d\nu \\ &= \langle R^2(t)\rangle H_R,\end{aligned}$$

where

$$\langle R^2(t)\rangle = \frac{12k_bT}{Nq^2\pi}\int_0^t dt'\int_0^\infty \frac{\sigma'(\nu)}{\nu}\sin(2\pi\nu t')d\nu, \tag{8}$$

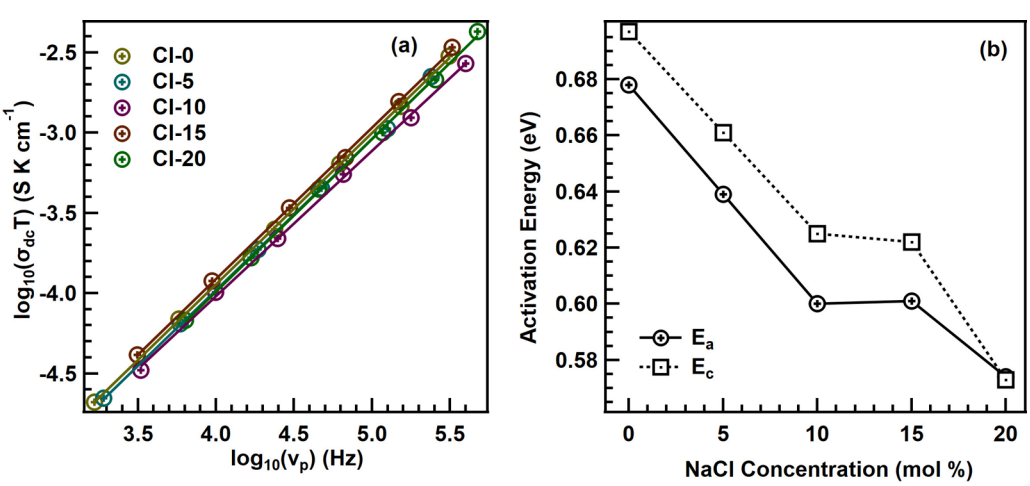

FIG. 9. (a) $\log_{10}(\sigma_{\mathrm{dc}}T)$ vs $\log_{10}(\nu_{\mathrm{p}})$ plot for different glass samples. (b) Activation energy for different NaCl concentration.

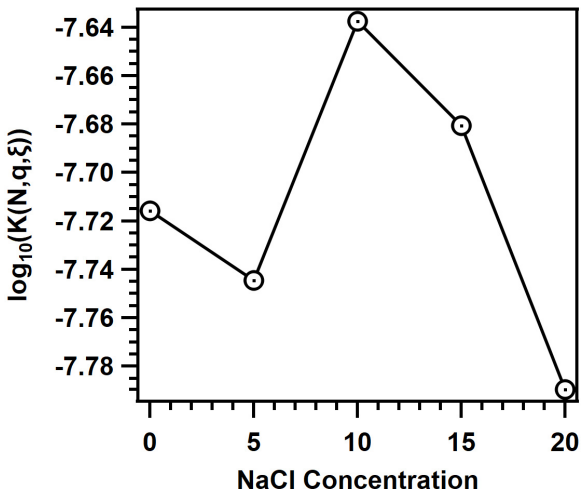

FIG. 10. Variation of $\log_{10}(\mathrm{K}(N,q,\xi))$ with respect to NaCl concentration.

$\langle R^2(t)\rangle$ is the mean-square displacement of the center of the charge of the mobile cations, and H_R is the Haven ratio. Generally, H_R depends on the ionic concentration of glasses and indicates the degree of correlation between two successive hops. Due to the lack of knowledge on H_R for the present glass system, we have calculated $\langle R^2(t)\rangle$ for all the glasses instead of $\langle r^2(t)\rangle$. Figure 11(a) show $\langle R^2(t)\rangle$ curves for all glasses at 398 K. Irrespective of the composition, $\langle R^2(t)\rangle$ curves obey the linear relation with time at longer timescales, i.e., $\langle R^2(t)\rangle \propto t$, whereas at a shorter timescale, $\langle R^2(t)\rangle$ curves obey the power-law time dependence, i.e., $\langle R^2(t)\rangle \propto t^{1-n}$. The variation of mean-square displacement $\langle R^2(t_p)\rangle$, calculated corresponding to the characteristic transition time t_p from short-range diffusion to long-range diffusion with NaCl concentrations, is shown in Fig. 11(b) for various temperatures. Irrespective of the temperature, $\langle R^2(t_p)\rangle$ decreases with increasing NaCl concentration up to 10 mol % and then increases with a further increase in NaCl concentration.

The spatial extent of the localized mobile cation is also calculated using the equation [85]

$$\langle R^2(t_\infty)\rangle = \frac{6k_b\varepsilon_o\Delta\varepsilon\, T}{Nq^2}, \tag{9}$$

where $\Delta\varepsilon = \varepsilon(s) - \varepsilon(\infty)$ is the dielectric strength of the material, where $\varepsilon(s)$ and $\varepsilon(\infty)$ are the static and high-frequency dielectric permittivity, respectively. Dielectric spectra [Fig. 8(b)] for the Cl-0 glass sample at different temperatures have been fitted with Eq. (10) [86] to extract the dielectric strength of the material,

$$\varepsilon'(\omega) = \varepsilon(\infty) + \frac{\varepsilon(s) - \varepsilon(\infty)\left[1 + (\omega\tau_{cc})^{1-\alpha}\sin\left(\frac{\pi\alpha}{2}\right)\right]}{1 + 2\left((\omega\tau_{cc})^{1-\alpha}\sin\left(\frac{\pi\alpha}{2}\right)\right) + (\omega\tau_{cc})^{2-2\alpha}} \tag{10}$$

where τ_{cc} is the characteristic relaxation time. With increasing NaCl concentration, both the values of $[\langle R^2(t_p)\rangle]^{1/2}$ and $[\langle R^2(t_\infty)\rangle]^{1/2}$, which are shown in Fig. 11(b), follow the same pattern. The increase in NaCl concentration decreases the value of $[\langle R^2(t_p)\rangle]^{1/2}$ and $[\langle R^2(t_\infty)\rangle]^{1/2}$ up to 10 mol % NaCl concentration, and then increases for a further addition of NaCl up to 20 mol %.

IV. DISCUSSION

In the comparison of the ^{27}Al MAS-NMR spectrum of Cl-0 glass with that of FS-6 glass, it is confirmed that the concentration of $\mathrm{Al(OP,F)_6}$ units increases with the addition of MoO_3. This observation can be explained considering the modifications in the Al/P ratio in the aluminophosphate network of the entire FS-6 glass network structure [32]. Raman spectra disclose that the addition of MoO_3 increases the P−O−Mo bonds. The formation of stable P−O−Mo bonds in multicomponent silicate glasses can be understood considering the concept of field strength ($= Z/r^2$, where Z is the charge of the cation and r is the average cation-anion bond distance) [87]. Due to the comparable field strength of P (2.13) and Mo (1.94 for tetrahedral and 1.54 for octahedral), the oxygen atom attracts both P and Mo equally and creates the P−O−Mo bonds. These P−O−Mo bonds decrease the concentration of phosphorus available for Al during the formation of an aluminophosphate network containing various $Q^n(m\mathrm{Al})$ units, where $m = 0 - 4$. Figure 2(a) shows the increase in $Q^0(2\mathrm{Al})$ units at the expense of $Q^0(3\mathrm{Al})$ units with the addition of NaCl, indicating that the Na^+ cations prefer to depolymerize the $Q^0(m\mathrm{Al})$ phosphorus tetrahedral units. It has been reported that the increase in the concentration of Na_2O in $AlPO_4$ glass increases the depolymerization of $Q^0(4\mathrm{Al})$ units through the following sequence: $Q^0(4\mathrm{Al}) \rightarrow Q^0(3\mathrm{Al}) \rightarrow Q^0(2\mathrm{Al}) \rightarrow Q^0(1\mathrm{Al})$ [62]. The increase in Na_2O in $AlPO_4$ glass further increases the aluminum coordination due to the creation of a large number of nonbridging oxygens. Therefore, it can be stated that the addition of MoO_3 to the FS-6 glass [32] creates P−O−Mo bonds, and the further addition of NaCl allows the sodium to create more nonbridging oxygens that enhance the concentration of $\mathrm{Al(OP)_6/Al(OP,F)_6}$ units.

Both Raman and MAS-NMR spectral analyses confirm that the progressive addition of NaCl to the Cl-0 glass influences the MoO_4, MoO_6, PO_4, AlO_4, and AlO_6 units. As discussed above, the variation in AlO_4 and AlO_6 units can be attributed to the formation of PO_4 units containing a large number of nonbridging oxygens and P−O−Mo bonds since the AlO_4 and AlO_6 units are solely connected to either PO_4 units or F atoms. This indicates that the increased concentration of sodium due to the addition of NaCl is interacting with the oxygen atoms connected to both Mo and P atoms. However, Raman spectra clearly indicate that the Mo−O−Mo bonds are absent. Therefore, we conclude that the MoO_4 units in the form of $\mathrm{Mo(=O)_2(OP)_2}$ and the MoO_6 units in the form of $\mathrm{Mo}(OP)_6$ are inserted in the aluminophosphate network [29,59]. Therefore, the interaction of sodium with MoO_4/MoO_6 may thus be limited by increasing the NaCl concentration in Cl-0 glass. It has been reported that the increase in the interaction of sodium with the MoO_6/MoO_4 units decreases the ^{23}Na chemical shift [59]. The ^{23}Na chemical shift relocates towards the higher chemical shift region with increasing NaCl in Cl-0 glass, further indicating that the sodium cations are interacting strongly with the PO_4 tetrahedral units compared with the MoO_6/MoO_4 units. Nev-

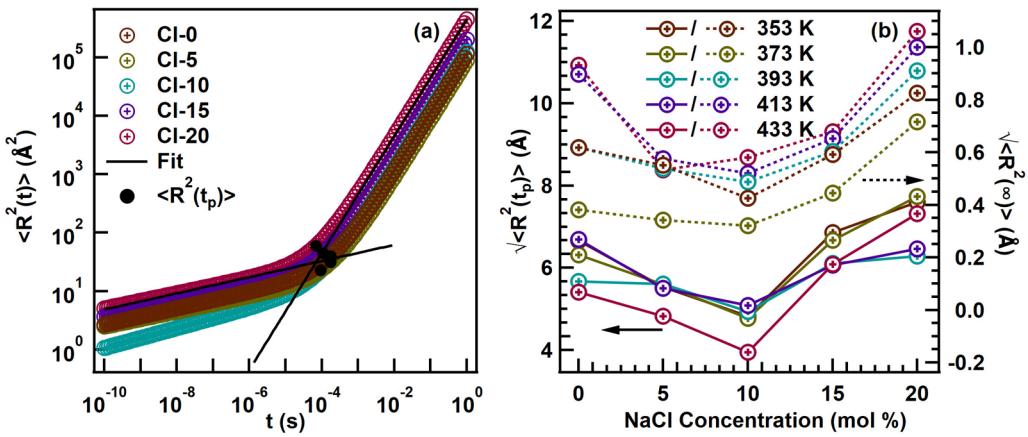

FIG. 11. (a) Mean-square displacement with respect to time for all glasses. (b) Characteristic displacement for different NaCl concentrations.

ertheless, the decrease in the Raman vibrational peak position for MoO_6/MoO_4 units with increasing NaCl may be due to the partial substitution of P with Na in the second coordination of MoO_6/MoO_4 units. It is known that the frequency of the vibrational units depends on the type of cation that connects with the terminal oxygen. For example, the substitution of Al^{3+} with Na^+ around the Q^0 phosphorus tetrahedral units shifts the Raman bands towards lower frequency due to the variation in the charge [56].

Several studies on aluminosilicate glasses have noted that the Cl^- ions are associated strongly with modifier cations [88,89]. It has been found that aluminum has no strong influence on the ^{35}Cl chemical environment, indicating a weak interaction between Al and Cl [88,89]. Therefore, since the Al−Cl bond formation is not common [89], the presence of Al-Cl linkages can be eliminated even in the present study, though the aluminophosphate and aluminosilicate glass systems are completely different. Nevertheless, we cannot completely rule out the existence of Al-Cl linkages because of the high concentration of NaCl in the present glass system. It should also be noted that, as is revealed from the ^{23}Na MAS-NMR spectra (Fig. 5), the solubility of NaCl is limited to 10 mol % in the Cl-0 glass system. The addition of a higher concentration of NaCl (>10 mol %) resulted in the presence of NaCl crystalline phases, which can even be observed in sodium silicate and aluminosilicate glasses due to the low solubility nature of NaCl [90,91].

The effective influence of dissolved NaCl on the bulk properties of glass depends on the bonding behavior of the Cl^- ion with the network structure. The dissolved Cl^- ion may not significantly affect the properties of glass if the Cl^- ion is bonded with the modifier cation, which is further surrounded by other Cl^- ions. In this case, the dissolved Cl^- ions form a Cl^--rich domain and function only as space fillers. On the other hand, homogeneously dispersed Cl^- anions, which are surrounded by the modifier cations that are further connected to the network structural units, such as PO_4 and AlO_4, significantly affect the properties of glass materials. It has been reported that an increase in the contribution of Cl^- in the coordination of Na increases the chemical shift in the ^{23}Na MAS-NMR spectra [19]. The positive shift of ^{23}Na NMR spectra (Fig. 5) upon increasing the addition of NaCl implies that the contribution of Cl^- ions in the coordination of Na is increasing. This confirms the homogeneous distribution of Cl^- ions in the present glass systems. Nevertheless, the formation of NaCl clusters cannot be ruled out after the addition of 10 mol % of NaCl since the ^{23}Na MAS-NMR spectra clearly show the presence of a crystalline phase. ^{31}P and ^{23}Na MAS-NMR spectra show that the major fraction of sodium cations are associated with the PO_4 tetrahedral units. The decrease in width of ^{31}P MAS-NMR spectra due to the disappearance of $Q^0(3Al)$ units with increasing NaCl concentration may indicate that Cl has an influence on the phosphorus environment through bonding with sodium. This highlights that the addition of NaCl could significantly enhance the ionic-conductivity of NaCl. The ionic-conductivity of Cl-0 glass is increased 2.4-fold (from 1.85×10^{-7} to 4.44×10^{-7} S/cm at 373 K) with the addition of 20 mol % of NaCl.

The increase in the concentration of Na−Cl bonds upon increasing the NaCl concentration should decrease the interlinkages between the aluminophosphate structural units [92]. This is because the large Cl^- ion is not directly connected to the aluminophosphate network. Therefore, the increase in molar volume with the increase in NaCl in the Cl-0 glass was expected. Nevertheless, the molar volume decreases (see Fig. S4 in the Supplemental Material) with NaCl concentration. This is possibly due to the destruction of the network skeleton and the formation of less directed bonds [93,94]. Moreover, the lower molar volume of NaCl (27 cm^3/mol) compared to that of Cl-0 glass (38 cm^3/mol) is also responsible for the decrease in molar volume upon increasing the addition of NaCl. The decrease in molar volume further indicates the decrease in interstitial space available, which in general influences the migration of mobile cations. The increase in conductivity despite a decrease in molar volume suggests that the average distance between hopping positions for Na^+ cations is decreasing with increasing NaCl concentration [95]. It has been reported that upon increasing the addition of polarizable Cl^- ions, the cation mobility and consequently the ionic-conductivity of the glasses increases [26,92]. Therefore, the increase in conductivity with increasing NaCl concentration could be attributed to the polarizability of Cl^- ions and the decreased hopping distance.

In ion-conducting glasses, dc conductivity follows the relation $\sigma = q\mu N$, where N is the concentration and μ is the mobility of the charge carriers. The values of $K(N,q,\xi)$ depend only on the concentration of the charge carrier. In Figs. 9(a) and 10, we have observed a variation in charge-carrier concentration with a variation in NaCl concentration. For glasses containing a higher concentration of NaCl (>10 mol %), the mobile cations responsible for the conductivity decrease. Nevertheless, the increase in ionic-conductivity confirms that the mobility of alkali cations plays a significant role in increasing NaCl concentration in the Cl-0 glass system.

The activation energy and mobility of any charge cation depends on its binding energy with the surrounding network as well as the network strength energy, and for larger cations such as sodium, the network strength energy is larger than the binding energy. We have observed a decreasing trend in the value of the activation energy, so this may indicate that the network strength energy is decreasing. Again, a decrease in the network strength energy usually increases the mobility of ions. This further confirms the depolymerization of the phosphate network.

In most of the glasses, $[\langle R^2(t_p)\rangle]^{1/2}$ depends inversely on dc conductivity. For example, $[\langle R^2(t_p)\rangle]^{1/2}$ is minimum for the highest conductive glass in yAg$_2$O-(1-y)[xSeO$_2$-(1-x)TeO$_2$] glass series [96]. This observation was explained based on the consideration that in the glass in which $[\langle R^2(t_p)\rangle]^{1/2}$ is lower, the mobile ions travel a lesser distance to overcome the force causing correlated forward-backward motion. We observe the same phenomena in Cl-0 glass containing a low NaCl concentration, i.e., NaCl (<10 mol %). The $[\langle R^2(t_p)\rangle]^{1/2}$ and $[\langle R^2(t_\infty)\rangle]^{1/2}$ decrease upon increasing the NaCl concentration up to 10 mol %, and then they increase with a further increase in NaCl concentration. This indicates that the increase in NaCl concentration increases the concentration of sodium cations responsible for the conductivity (Figs. 10 and 11) and decreases the distance between the two ions. Therefore, the mobile ion takes a lesser distance to overcome the force causing correlated forward-backward motion, which shows the decreasing trend in the value of $[\langle R^2(t_p)\rangle]^{1/2}$ and $[\langle R^2(t_\infty)\rangle]^{1/2}$. In glasses containing a higher NaCl concentration (NaCl >10 mol %), though the concentration of charge carriers decreases and the value of $[\langle R^2(t_p)\rangle]^{1/2}$ and $[\langle R^2(t_\infty)\rangle]^{1/2}$ increases, the conductivity still increases. This opposite phenomenon contradicts the observations in most of the glasses. The formation of nonbridging oxygens in glasses depolymerizes the network structure and decreases the value of $[\langle R^2(t_p)\rangle]^{1/2}$ because of the reduced hopping distances of mobile cations. $[\langle R^2(t_p)\rangle]^{1/2}$ is also dependent on the interionic Coulombic interactions. The Coulomb interaction depends on the number of charged ions present in the system. In the current system (for NaCl concentration >10 mol %), a decrease in charge-carrier concentration (Fig. 10) also indicates a tendency to decrease the Coulomb interaction. This ensures that sodium-ion mobility, as well as conductivity, is further increased. In the present glass systems, the increase in P−O−Mo bonds as well as the increase in Q^0(2Al) units at the expense of Q^0(3Al) units indicates the creation of more nonbridging oxygens with increasing NaCl concentration. These nonbridging oxygens should decrease the value of $[\langle R^2(t_p)\rangle]^{1/2}$ and further increase the conductivity. Nevertheless, the creation of the shallower potential energy landscape for the sodium cations due to the interaction with the Cl^- ions at higher NaCl concentration (>10 mol %) might be responsible for the increase in the mobility of sodium ions and consequently the conductivity. Sklepić, Tricot, Mošner, Koudelka, and Moguš-Milanković [97] observed a similar trend where conductivity as well as $[\langle R^2(t_p)\rangle]^{1/2}$ increased for the $Na_2O-P_2O_5-GeO_2$ glass system. They identified this as a modification of the network structure surrounding the Na^+ ions. Therefore, in the present study, the increase in the conductivity of Cl glasses is strongly due to the enhancement in the mobility of sodium as a result of structural changes in the glasses.

V. CONCLUSIONS

The addition of NaCl in the glass system (31.725 Na_2O-12.69 Al_2O_3-31.725 P_2O_5-8.46 NaF-5.40 Na_2SO_4-10 MoO_3) enhances ionic-conductivity with changing structure and sodium ion dynamics. The ionic-conductivity of base glass increases by 2.4 times (from 1.85×10^{-7} to 4.44×10^{-7} S/cm at 373 K) with the addition of 20 mol % of NaCl. MAS-NMR spectra reveal that the solubility limit of NaCl is limited to 10 mol %, and a higher concentration of NaCl >10 mol % resulted in the presence of NaCl crystalline phases. Raman spectra confirm that the addition of MoO_3 increases the P−O−Mo bonds and allows the sodium to create more nonbridging oxygens, which enhances the concentration of Al(OP, F)$_6$ units. They also reveal that Mo−O−Mo bonds are absent in this glass system. The variation of $\log_{10}(K(N,q,\xi))$ with NaCl concentration reveals that the sodium ion participating in the conductivity increases with increasing NaCl concentration up to 10 mol % and then decreases. The characteristic displacement curve indicates that for high concentrations of NaCl (>10 mol %), the sodium ion mobility increases due to a decrease in Coulombic interaction as well as an increase in the number of nonbridging oxygens. Therefore, in the current glass system, Na-ion concentration in low NaCl-containing (<10 mol %) glasses and Na-ion mobility in high NaCl-containing (>10 mol %) glasses play a major role in improving ionic-conductivity.

ACKNOWLEDGMENTS

This work was developed under the framework of the project funded by the Science and Engineering Research Board (SERB), DST, Govt. of India, through the Early Career Research Award (ECR/2018/000292). I.M. and A.R.A. acknowledge the financial support by DST-SERB (ECR/2018/000292). L.L. and K.K.D. acknowledge CAR (Centre Advance Research), Dr. HarisinghGour University, for providing a Solid-State NMR facility. M.G. is thankful for the IOE-BHU grant [DEV.scheme.no.6031(B)]. A.G. acknowledges SERB for the J. C. Bose Fellowship (Grant No. SB/S2/JCB-33/2014).

[1] H. H. Heenen, J. Voss, C. Scheurer, K. Reuter, and A. C. Luntz, Multi-ion conduction in Li_3OCl glass electrolytes, J. Phys. Chem. Lett. **10**, 2264 (2019).

[2] X. Miao, H. Wang, R. Sun, C. Wang, Z. Zhang, Z. Li, and L. Yin, Interface engineering of inorganic solid-state electrolytes for high-performance lithium metal batteries, Energy Environ. Sci. **13**, 3780 (2020).

[3] H. Nagata and J. Akimoto, Excellent deformable oxide glass electrolytes and oxide-type all-solid-state Li_2-Si batteries employing these electrolytes, ACS Appl. Mater. Interfaces **13**, 35785 (2021).

[4] M. H. Braga, A. J. Murchison, J. E. Oliveira, and J. B. Goodenough, Low-temperature performance of a ferroelectric glass electrolyte rechargeable cell, ACS Appl. Energy Mater. **2**, 4943 (2019).

[5] M. V. Reddy, C. M. Julien, A. Mauger, and K. Zaghib, Sulfide and oxide inorganic solid electrolytes for all-solid-state Li batteries: A review, Nanomaterials **10**, 1606 (2020).

[6] D. Park, K. Kim, G. H. Chun, B. C. Wood, J. H. Shim, and S. Yu, Materials design of sodium chloride solid electrolytes $Na_3MCl)6$ for all-solid-state sodium-ion batteries, J. Mater. Chem. A **9**, 23037 (2021).

[7] H. Park, S. Yu, and D. J. Siegel, Predicting charge transfer stability between sulfide solid electrolytes and Li metal anodes, ACS Energy Lett. **6**, 150 (2021).

[8] Y. Xiao, Y. Wang, S.-H. Bo, J. C. Kim, L. J. Miara, and G. Ceder, Understanding interface stability in solid-state batteries, Nat. Rev. Mater. **5**, 105 (2020).

[9] V. C. V. Gowda, B. K. Chethana, and C. N. Reddy, Ion transport studies in lithium phospho-molybdate glasses containing Cl− ion, Mater. Sci. Eng. B **178**, 826 (2013).

[10] F. Muñoz, J. Ren, L. van Wüllen, T. Zhao, H. Kirchhain, U. Rehfuß, and T. Uesbeck, Structure and dynamics of LiPON and NaPON oxynitride phosphate glasses by solid-state NMR, J. Phys. Chem. C **125**, 4077 (2021).

[11] B. Poletto Rodrigues, R. Limbach, G. Buzatto de Souza, H. Ebendorff-Heidepriem, and L. Wondraczek, Correlation between ionic mobility and plastic flow events in $NaPo_3$-NaCl-Na_2SO_4 glasses, Front. Mater. **6** 128, (2019).

[12] Z. Zhang, J. Ren, and L. Hu, Fast ionic conducting glasses in the system 20LiCl-40Li_2O-(80-x)$PO_{5/2}$-XMoO_3: The structural dependence of ion conductivity studied by solid-state nuclear magnetic resonance spectroscopy, J. Phys. Chem. C **124**, 6528 (2020).

[13] G. Tricot, K. Ben Tayeb, L. Koudelka, P. Mosner, and H. Vezin, Insertion of MoO_3 in borophosphate glasses investigated by magnetic resonance spectroscopies, J. Phys. Chem. C **120**, 9443 (2016).

[14] E. R. Andrew, A. Bradbury, and R. G. Eades, Removal of dipolar broadening of nuclear magnetic resonance spectra of solids by specimen rotation, Nature (London) **183**, 1802 (1959).

[15] H. Eckert, Network former mixing (NFM) effects in ion-conducting glasses - Structure/property correlations studied by modern solid-state NMR techniques, Diffus. Found. **6**, 144 (2016).

[16] L. van Wüllen, G. Tricot, and S. Wegner, An advanced NMR protocol for the structural characterization of aluminophosphate glasses, Solid State Nucl. Magn. Reson. **32**, 44 (2007).

[17] V. R. Seymour, J. M. Griffin, B. E. Griffith, S. J. Page, D. Iuga, J. V. Hanna, and M. E. Smith, Improved understanding of atomic ordering in $Y_4SixAl_{2-x}O_{9-X}Nx$ materials using a combined solid-state NMR and computational approach, J. Phys. Chem. C **124**, 23976 (2020).

[18] E. Winter, P. Seipel, V. Miß, S. Spannenberger, B. Roling, and M. Vogel, 7Li NMR studies of short-range and long-range lithium ion dynamics in a heat-treated lithium iodide-doped lithium thiophosphate glass featuring high ion conductivity, J. Phys. Chem. C **124**, 28614 (2020).

[19] Y. Ogiwara, K. Echigo, and M. Hanaya, Formation of amorphous licl aggregate regions in LiCl-Li_2O-P_2O_5 fast ion conducting glasses studied by ac conductometry and 7Li MAS NMR, J. Non. Cryst. Solids **352**, 5192 (2006).

[20] S. Spannenberger *et al.*,, Annealing-induced vacancy formation enables extraordinarily high Li+ ion conductivity in the amorphous electrolyte 0.33 $LiI_{+0.67}$ Li_3PS_4, Solid State Ion. **341**, 115040 (2019).

[21] A. Krishnamurthy, T. Nguyen, M. Fayek, B. Shabaga, and S. Kroeker, Network structure and dissolution properties of phosphate-doped borosilicate glasses, J. Phys. Chem. C **124**, 21184 (2020).

[22] J. A. Duffy and M. D. Ingram, An interpretation of glass chemistry in terms of the optical basicity concept, J. Non. Cryst. Solids **21**, 373 (1976).

[23] L. Bih, M. El Omari, J. M. Réau, A. Nadiri, A. Yacoubi, and M. Haddad, Electrical properties of glasses in the Na_2O-MoO_3-P_2O_5 system, Mater. Lett. **50**, 308 (2001).

[24] S. Renka, L. Pavić, G. Tricot, P. Mošner, L. Koudelka, A. Moguš-Milanković, and A. Šantić, A significant enhancement of sodium ion conductivity in phosphate glasses by addition of WO_3 and MoO_3: The effect of mixed conventional–conditional glass-forming oxides, Phys. Chem. Chem. Phys. **23**, 9761 (2021).

[25] J. C. Bazan, J. A. Duffy, M. D. Ingram, and M. R. Mallace, Conductivity anomalies in tungstate-phosphate glasses: Evidence for an ion-polaron interaction?, Solid State Ion. **86–88**, 497 (1996).

[26] R. Prasada Rao, T. D. Tho, and S. Adams, Lithium ion transport pathways in XLiCl-(1-x)(0.6Li_2O-0.4P_2O_5) glasses, J. Power Sources **189**, 385 (2009).

[27] R. Prasada Rao and M. Seshasayee, Molecular dynamics simulation of ternary glasses Li_2O-P_2O_5-LiCl, Solid State Commun. **131**, 537 (2004).

[28] J. P. Malugani and G. Robert, Conductivite ionique dans les verres $LiPO_3$LiX (X = I, Br, Cl), Mater. Res. Bull. **14**, 1075 (1979).

[29] J. A. Davies, M. Mugglestone, S. Yang, and A. M. Ellis, IR spectroscopy of the cesium iodide–water complex, J. Phys. Chem. A **124**, 6528 (2020).

[30] H. Jia, X. Liang, T. An, L. Peng, J. Feng, and J. Xie, Effect of halogen doping in sodium solid electrolytes based on the Na–Sn–Si–P–S quinary system, Chem. Mater. **32**, 4065 (2020).

[31] X. Feng, P.-H. Chien, Z. Zhu, I.-H. Chu, P. Wang, M. Immediato-Scuotto, H. Arabzadeh, S. P. Ong, and Y.-Y. Hu, Studies of functional defects for fast Na-ion conduction in $Na_{3-y}PS_4$-xCl_x with a combined experimental and computational approach, Adv. Funct. Mater. **29**, 1807951 (2019).

[32] I. Mandal, S. Chakraborty, K. Jayanthi, M. Ghosh, K. K. Dey, K. Annapurna, J. Mukhopadhyay, A. Das Sharma, and A. R.

Allu, Role of sodium-ion dynamics and characteristic length scales in ion conductivity in aluminophosphate glasses containing Na_2SO_4, J. Phys. Chem. C **126**, 3276 (2022).

[33] I. Mandal, S. Chakraborty, K. Annapurna, A. Das Sharma, J. Mukhopadhyay, and A. R. Allu, Understanding the sodium-ion dynamics in NASICON ($Na_3Al_2P_3O_{12}$) glass containing NaF: scaling of electrical conductivity spectra, J. Alloys Compd. **885**, 160952 (2021).

[34] N. S. Tagiara, D. Palles, E. D. Simandiras, V. Psycharis, A. Kyritsis, and E. I. Kamitsos, Synthesis, thermal and structural properties of pure TeO_2 glass and zinc-tellurite glasses, J. Non. Cryst. Solids **457**, 116 (2017).

[35] W. T. Dixon, Spinning-sideband-free and Spinning-sideband-only NMR spectra in spinning samples, J. Chem. Phys. **77**, 1800 (1982).

[36] O. N. Antzutkin, S. C. Shekar, and M. H. Levitt, Two-dimensional sideband separation in magic-angle-spinning NMR, J. Magn. Res. Ser. A **115**, 7 (1995).

[37] See Supplemental Material at http://link.aps.org/supplemental/10.1103/PhysRevMaterials.6.115403 for further experimental details and supplementary figures.

[38] W. S. Veeman, Carbon-13 chemical shift anisotropy, Prog. Nucl. Magn. Res. Spectrosc. **16**, 193 (1984).

[39] J. A. Pople, Nuclear magnetic resonance in diamagnetic materials. The theory of chemical shifts, Discuss. Faraday Soc. **34**, 7 (1962).

[40] R. J. Levitt, Y. Zhao, M.-J. Blouin, and M. Pollak, The hedgehog pathway inhibitor cyclopamine increases levels of P27 and decreases both expression of IGF-II and activation of Akt in PC-3 prostate cancer cells, Cancer Lett. **255**, 300 (2007).

[41] N. Ivchenko, C. E. Hughes, and M. H. Levitt, Application of cogwheel phase cycling to sideband manipulation experiments in solid-state NMR, J. Magn. Reson. **164**, 286 (2003).

[42] J. Herzfeld and A. E. Berger, Sideband intensities in NMR spectra of samples spinning at the magic angle, J. Chem. Phys. **73**, 6021 (1980).

[43] M. Ghosh, S. Sadhukhan, and K. K. Dey, Elucidating the internal structure and dynamics of A−chitin by 2DPASS-MAS-NMR and spin-lattice relaxation measurements, Solid State Nucl. Magn. Reson. **97**, 7 (2019).

[44] K. K. Dey, M. M. Deshmukh, and M. Ghosh, A description of the local structure and dynamics of ketoconazole molecule by solid-state NMR measurements and DFT calculations: Proposition for NMR crystallography, ChemistrySelect **6**, 10208 (2021).

[45] K. K. Dey, L. Lodhi, and M. Ghosh, Study of the variation of the electronic distribution and motional dynamics of two independent molecules of an asymmetric unit of atorvastatin calcium by solid-state NMR measurements, ACS Omega **6**, 22752 (2021).

[46] R. Bhowal, A. A. Balaraman, M. Ghosh, S. Dutta, K. K. Dey, and D. Chopra, Probing atomistic behavior to unravel dielectric phenomena in charge transfer cocrystals, J. Am. Chem. Soc. **143**, 1024 (2021).

[47] M. Engelsberg and R. E. Norberg, Nuclear magnetic resonance and nuclear-spin dynamics in InP, Phys. Rev. B **5**, 3395 (1972).

[48] J. W. Zwanziger, J. C. McLaughlin, and S. L. Tagg, Sodium distribution in sodium tellurite glasses probed with spin-echo NMR, Phys. Rev. B **56**, 5243 (1997).

[49] J. Haase and E. Oldfield, Spin-echo behavior of nonintegral-spin quadrupolar nuclei in inorganic solids, J. Magn. Reson. Ser. A **101**, 30 (1993).

[50] L. Koudelka, I. Rösslerová, J. Holubová, P. Mošner, L. Montagne, and B. Revel, Structural study of PbO-MoO_3-P_2O_5 glasses by raman and NMR spectroscopy, J. Non. Cryst. Solids **357**, 2816 (2011).

[51] J. Šubčík, L. Koudelka, P. Mošner, L. Montagne, B. Revel, and I. Gregora, Structure and properties of MoO_3-containing zinc borophosphate glasses, J. Non. Cryst. Solids **355**, 970 (2009).

[52] J. Šubčík, L. Koudelka, P. Mošner, L. Montagne, G. Tricot, L. Delevoye, and I. Gregora, Glass-forming ability and structure of ZnO-MoO_3-P_2O_5 glasses, J. Non. Cryst. Solids **356**, 2509 (2010).

[53] J. Nikolić, L. Pavić, A. Šantić, P. Mošner, L. Koudelka, D. Pajić, and A. Moguš-Milanković, Novel insights into electrical transport mechanism in ionic-polaronic glasses, J. Am. Ceram. Soc. **101**, 1221 (2018).

[54] A. Chatterjee, S. Majumdar, and A. Ghosh, Effect of network structure on dynamics of lithium ions in molybdenum phosphate mixed former glasses, Solid State Ion. **347**, 115238 (2020).

[55] A. Moguš-Milanković, A. Gajović, A. Šantić, and D. E. Day, Structure of sodium phosphate glasses containing Al_2O_3 and/or Fe_2O_3. Part I, J. Non-Cryst. Solids **289**, 204 (2001).

[56] B. N. Nelson and G. J. Exarhos, Vibrational spectroscopy of cation-site interactions in phosphate glasses, J. Chem. Phys. **71**, 2739 (1979).

[57] D. Möncke *et al.*, $NaPO_3$-AlF_3 glasses: Fluorine evaporation during melting and the resulting variations in structure and properties, J. Chem. Technol. Metall. **53**, 1047 (2018).

[58] B. V. R. Chowdari, K. L. Tan, and W. T. Chia, Structural and physical characterization of Li_2O:P_2O_5:MO_3 (M = Cr_2, Mo, W) ion conducting glasses, MRS Proc. **293**, 325 (1992).

[59] S. H. Santagneli, C. C. de Araujo, W. Strojek, H. Eckert, G. Poirier, S. J. L. Ribeiro, and Y. Messaddeq, Structural studies of $NaPO_3$-MoO_3 glasses by solid-state nuclear magnetic resonance and raman spectroscopy, J. Phys. Chem. B **111**, 10109 (2007).

[60] B. Raguenet, G. Tricot, G. Silly, M. Ribes, and A. Pradel, Revisiting the 'Mixed glass former Effect' in ultra-fast quenched borophosphate glasses by advanced 1D/2D solid state NMR, J. Mater. Chem. **21**, 17693 (2011).

[61] S. R. Keshri *et al.*, Ionic conductivity of $Na_3Al_2P_3O_{12}$ glass electrolytes—role of charge compensators, Inorg. Chem. **60**, 12893 (2021).

[62] L. Zhang and H. Eckert, Short- and medium-range order in sodium aluminophosphate glasses: New insights from high-resolution dipolar solid-state NMR spectroscopy, J. Phys. Chem. B **110**, 8946 (2006).

[63] C. C. de Araujo, W. Strojek, L. Zhang, H. Eckert, G. Poirier, S. J. L. Ribeiro, and Y. Messaddeq, Structural studies of $NaPO_3$–WO_3 glasses by solid state NMR and raman spectroscopy, J. Mater. Chem. **16**, 3277 (2006).

[64] L. Zhang, C. C. de Araujo, and H. Eckert, Structural role of fluoride in aluminophosphate Sol−Gel glasses: High-resolution double-resonance NMR studies, J. Phys. Chem. B **111**, 10402 (2007).

[65] M. Blais-Roberge, S. H. Santagneli, S. H. Messaddeq, M. Rioux, Y. Ledemi, H. Eckert, and Y. Messaddeq, Structural

characterization of AgI–$AgPO_3$–Ag_2WO_4 superionic conducting glasses by advanced solid-state NMR techniques, J. Phys. Chem. C **121**, 13823 (2017).

[66] F. Behrends and H. Eckert, Mixed-alkali effects in aluminophosphate glasses: a re-examination of the system $[XNa_2O(1–x)Li_2O]_{0.46}[YAl_2O_3(1–y)P_2O_5]_{0.54}$, J. Phys. Chem. C **115**, 17175 (2011).

[67] R. K. Brow, R. J. Kirkpatrick, and G. L. Turner, Nature of alumina in phosphate glass: II, structure of sodium alurninophosphate glass, J. Am. Ceram. Soc. **76**, 919 (1993).

[68] L. Zhang, C. C. de Araujo, and H. Eckert, a new Sol−Gel route to aluminum fluoride phosphate glasses: Mechanistic investigations by NMR spectroscopy, Chem. Mater. **17**, 3101 (2005).

[69] D. Mohr, A. S. S. de Camargo, C. C. de Araujo, and H. Eckert, Local environment of scandium in aluminophosphate laser glasses: structural studies by solid state NMR spectroscopy, J. Mater. Chem. **17**, 3733 (2007).

[70] X. Xu and R. J. Kirkpatrick, NaCl interaction with interfacially polymerized polyamide films of reverse osmosis membranes: A solid-state 23Na NMR study, J. Memb. Sci. **280**, 226 (2006).

[71] R. K. Brow, R. J. Kirkpatrick, and G. L. Turner, The short range structure of sodium phosphate glasses I. MAS NMR studies, J. Non-Cryst. Solids **116**, 39 (1990).

[72] I. Mandal, S. Chakraborty, M. Ghosh, K. K. Dey, K. Annapurna, and A. R. Allu, Structure and conductivity correlation in NASICON based $Na_3Al_2P_3O_{12}$ glass: Effect of Na_2SO_4, Front. Mater. **8**, 802379 (2022).

[73] S. Prabakar, R. M. Wenslow, and K. T. Mueller, Structural properties of sodium phosphate glasses from $^{23}Na \rightarrow {}^{31}P$ cross-polarization NMR, J. Non-Cryst. Solids **263–264**, 82 (2000).

[74] B. Gee and H. Eckert, Cation distribution in mixed-alkali silicate glasses. NMR studies by $^{23}Na-\{^{7}Li\}$ and $^{23}Na-\{^{6}Li\}$ spin echo double resonance, J. Phys. Chem. **100**, 3705 (1996).

[75] E. Ratai, J. C. C. Chan, and H. Eckert, Local coordination and spatial distribution of cations in mixed-alkali borate glasses, Phys. Chem. Chem. Phys. **4**, 3198 (2002).

[76] Y. Yu, B. Stevensson, and M. Edén, Structural role of sodium in borosilicate, phosphosilicate, and borophosphosilicate glasses unveiled by solid-state NMR and MD simulations, J. Phys. Chem. C **123**, 25816 (2019).

[77] B. Gee and H. Eckert, ^{23}Na Nuclear magnetic resonance spin echo decay spectroscopy of sodium silicate glasses and crystalline model compounds, Solid State Nucl. Magn. Reson. **5**, 113 (1995).

[78] S. W. Martin, R. Christensen, G. Olson, J. Kieffer, and W. Wang, New interpretation of Na+-ion conduction in and the structures and properties of sodium borosilicate mixed glass former glasses, J. Phys. Chem. C **123**, 5853 (2019).

[79] A. S. Nowick and B. S. Lim, Electrical relaxations: Simple versus complex ionic systems, Phys. Rev. B **63**, 184115 (2001).

[80] D. M. Laughman, R. D. Banhatti, and K. Funke, New nearly constant loss feature detected in glass at low temperatures, Phys. Chem. Chem. Phys. **12**, 14102 (2010).

[81] D. L. Sidebottom, Dimensionality Dependence of the Conductivity Dispersion in Ionic Materials, Phys. Rev. Lett. **83**, 983 (1999).

[82] D. L. Sidebottom, Colloquium: Understanding ion motion in disordered solids from impedance spectroscopy scaling, Rev. Mod. Phys. **81**, 999 (2009).

[83] B. P. Rodrigues, H. Ebendorff-Heidepriem, and L. Wondraczek, Decoupling mobility and charge carrier concentration in AgR-AgPO3 glasses (R = Cl, Br, I), Solid State Ion. **334**, 99 (2019).

[84] R. Kubo, Statistical-mechanical theory of irreversible processes. I. General theory and simple applications to magnetic and conduction problems, J. Phys. Soc. Jpn. **12**, 570 (1957).

[85] A. Shaw and A. Ghosh, Dynamics of lithium ions in borotellurite mixed former glasses: Correlation between the characteristic length scales of mobile ions and glass network structural units, J. Chem. Phys. **141**, 164504 (2014).

[86] K. S. Cole and R. H. Cole, Dispersion and absorption in dielectrics I. Alternating current characteristics, J. Chem. Phys. **9**, 341 (1941).

[87] A. Krishnamurthy and S. Kroeker, Improving molybdenum and sulfur vitrification in borosilicate nuclear waste glasses using phosphorus: Structural insights from NMR, Inorg. Chem. **61**, 73 (2022).

[88] J. F. Stebbins and L.-S. Du, Chloride ion sites in silicate and aluminosilicate glasses: A preliminary study by ^{35}Cl solid-state NMR, Am. Mineral. **87**, 359 (2002).

[89] T. O. Sandland, L.-S. Du, J. F. Stebbins, and J. D. Webster, Structure of cl-containing silicate and aluminosilicate glasses: A ^{35}Cl MAS-NMR study, Geochim. Cosmochim. Acta **68**, 5059 (2004).

[90] J. D. Webster and B. De Vivo, Experimental and modeled solubilities of chlorine in aluminosilicate Melts, consequences of magma evolution, and implications for exsolution of hydrous chloride melt at Mt. Somma-vesuvius, Am. Mineral. **87**, 1046 (2002).

[91] S. M. Thornber, L. M. Mottram, A. R. Mason, P. Thompson, M. C. Stennett, and N. C. Hyatt, Solubility, speciation and local environment of chlorine in zirconolite glass–ceramics for the immobilisation of plutonium residues, RSC Adv. **10**, 32497 (2020).

[92] A. V. Deshpande and V. K. Deshpande, Influence of LiCl addition on the electrical conductivity of $Li_2O/B_2O_3/SiO_2$ glass system, Solid State Ion. **154–155**, 433 (2002).

[93] R. Zhou, C. Calahoo, Y. Ding, X. Yang, C. P. Romao, and L. Wondraczek, Structural origin of the optical properties of ag-doped fluorophosphate and sulfophosphate glasses, J. Phys. Chem. B **125**, 637 (2021).

[94] I. Kansal, D. U. Tulyaganov, A. Goel, M. J. Pascual, and J. M. F. Ferreira, Structural analysis and thermal behavior of diopside–fluorapatite–wollastonite-based glasses and glass–ceramics, Acta Biomater. **6**, 4380 (2010).

[95] F. Moreau, A. Durán, and F. Muñoz, Structure and properties of high Li_2O-containing aluminophosphate glasses, J. Eur. Ceram. Soc. **29**, 1895 (2009).

[96] A. Palui and A. Ghosh, Structure-transport correlation of superionic mixed network former glasses, Solid State Ion. **343**, 115126 (2019).

[97] K. Sklepić, G. Tricot, P. Mošner, L. Koudelka, and A. Moguš-Milanković, Sodium ion conductivity in mixed former Na_2O-P_2O_5-GeO_2 and Na_2O-B_2O_3-P_2O_5-GeO_2 glasses, J. Phys. Chem. C **125**, 10593 (2021).